

Figure SM1. Individual DSC-TGA thermograms of the solid phases PGZ·HCl-FLV (1:1) prepared by NG or LAG solvent-screening. Also, individual DSC-TGA thermograms of pure PGZ·HCl and FLV.

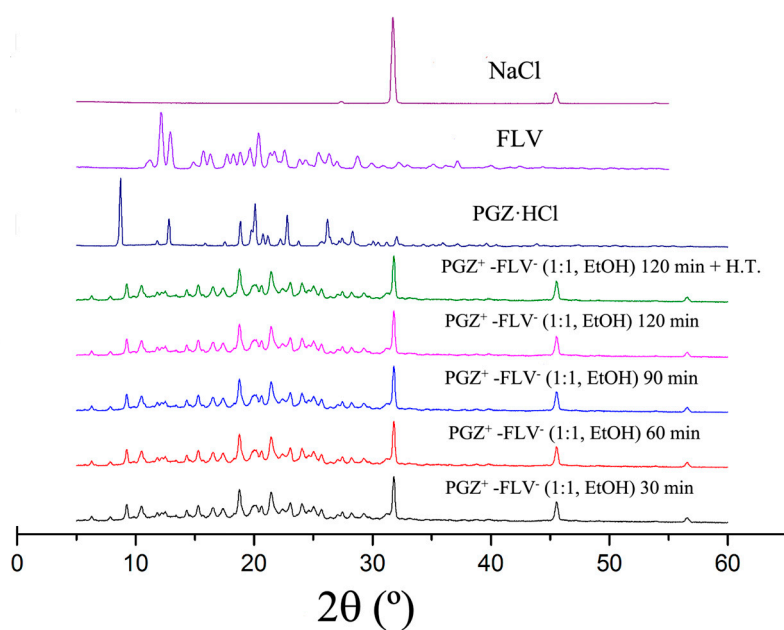


Figure SM2. Diffractograms of the salt PGZ⁺·FLV⁻ (1:1, EtOH) extending the reaction times

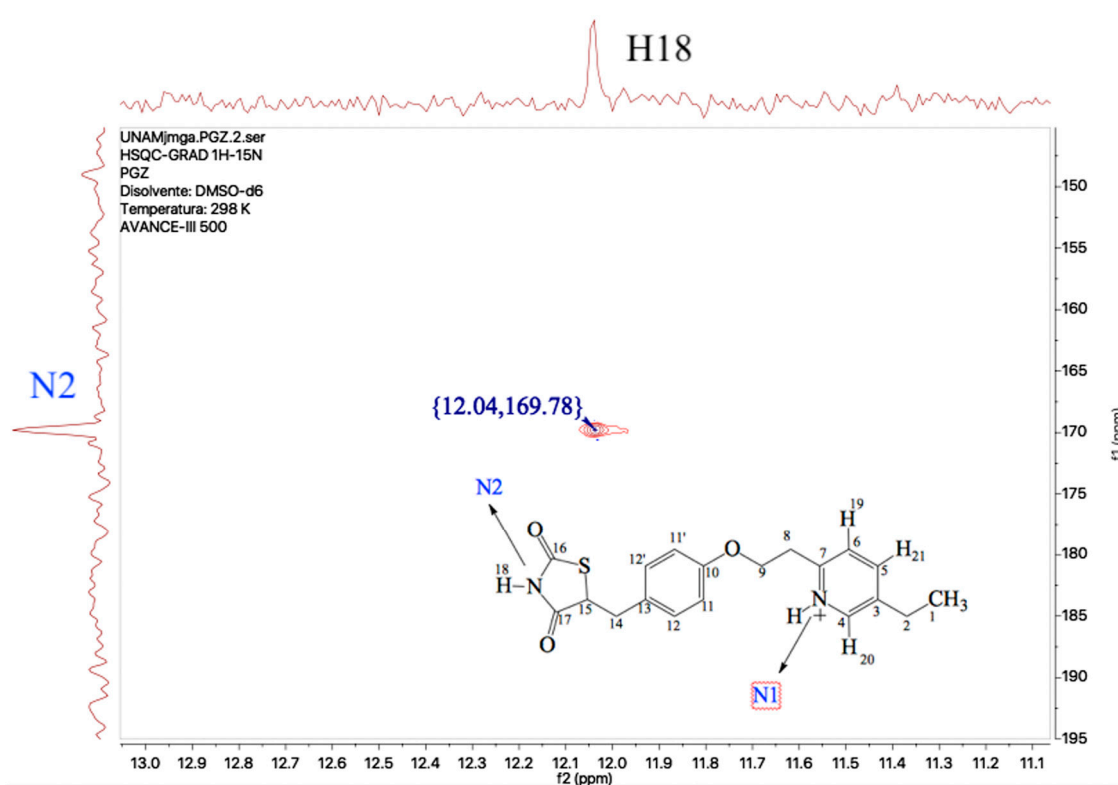


Figure SM3. HSQC ¹H-¹⁵N NMR spectrum of PGZ·HCl in d₆-DMSO

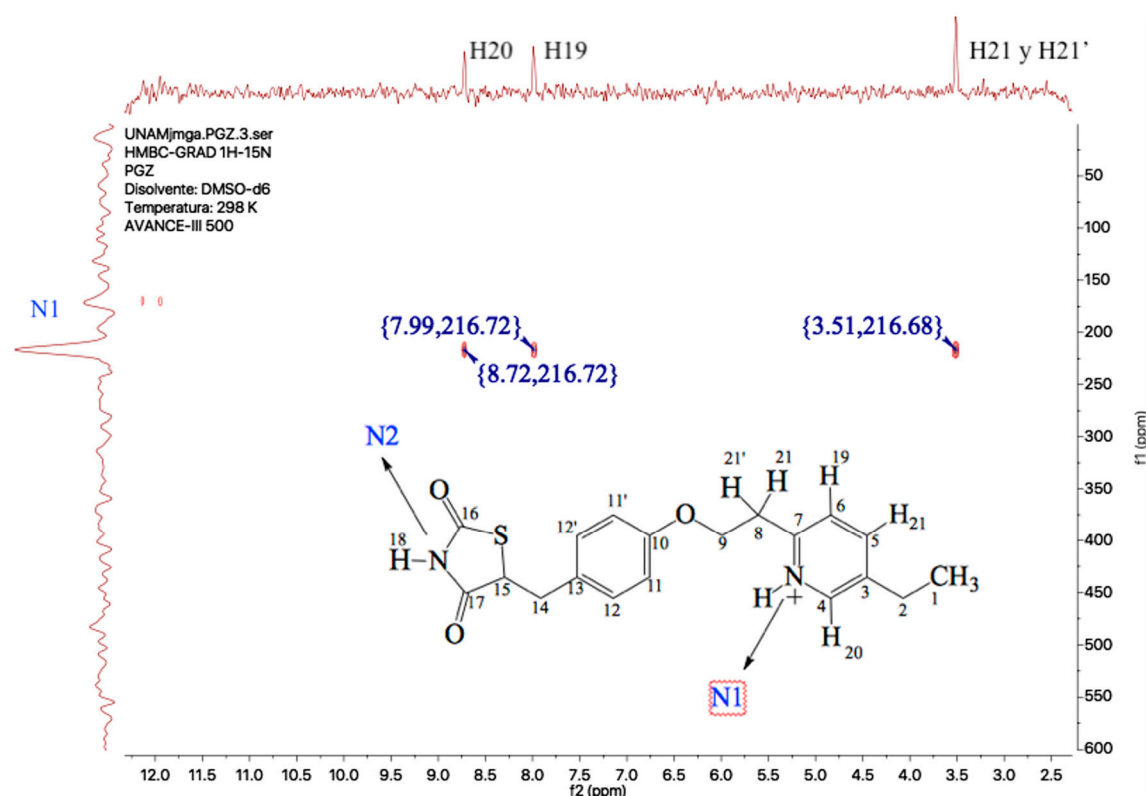
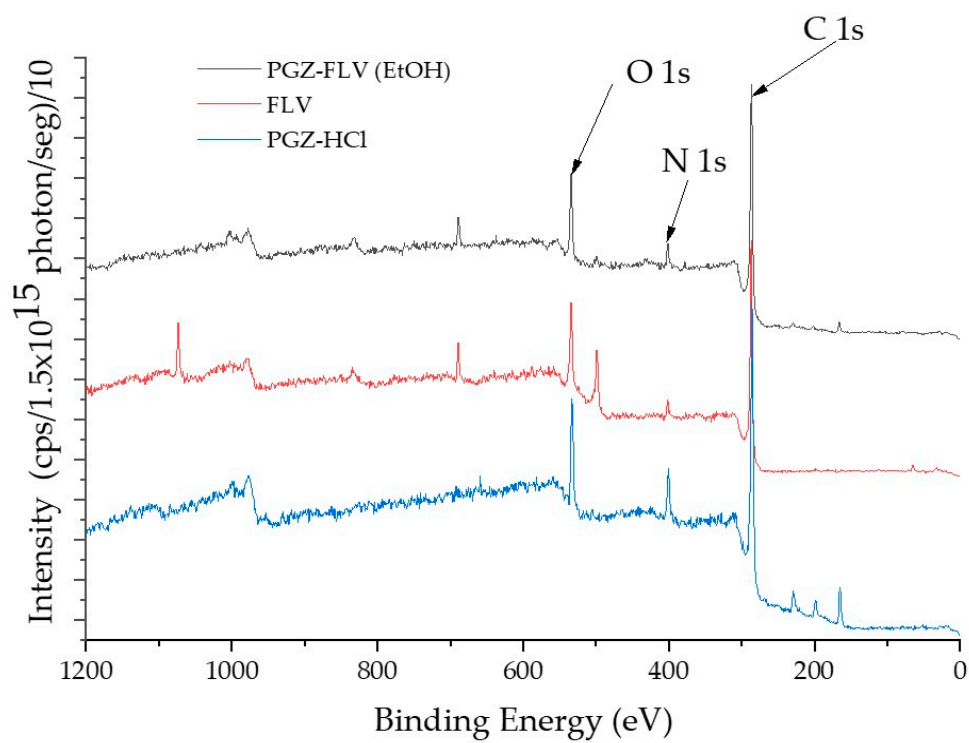


Figure SM4. HMBC ^1H - ^{15}N NMR spectrum of PGZ·HCl in d_6 -DMSO



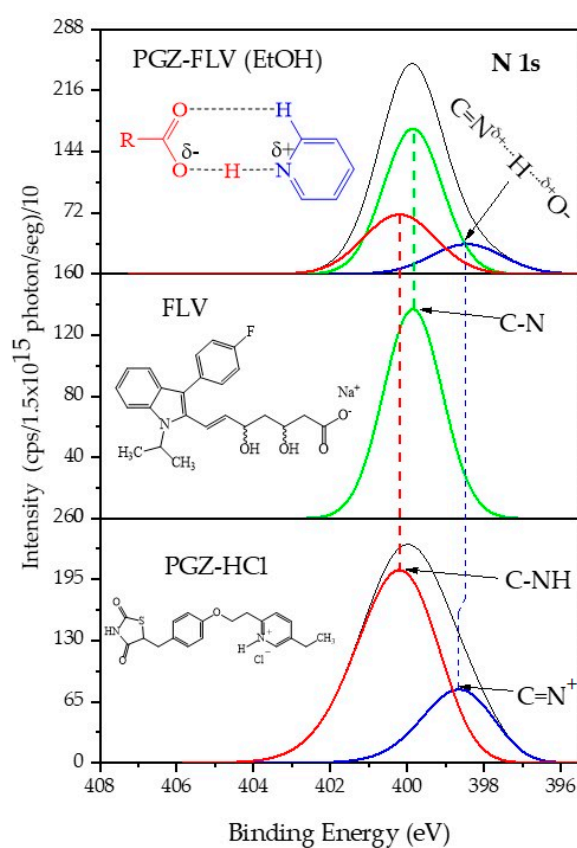
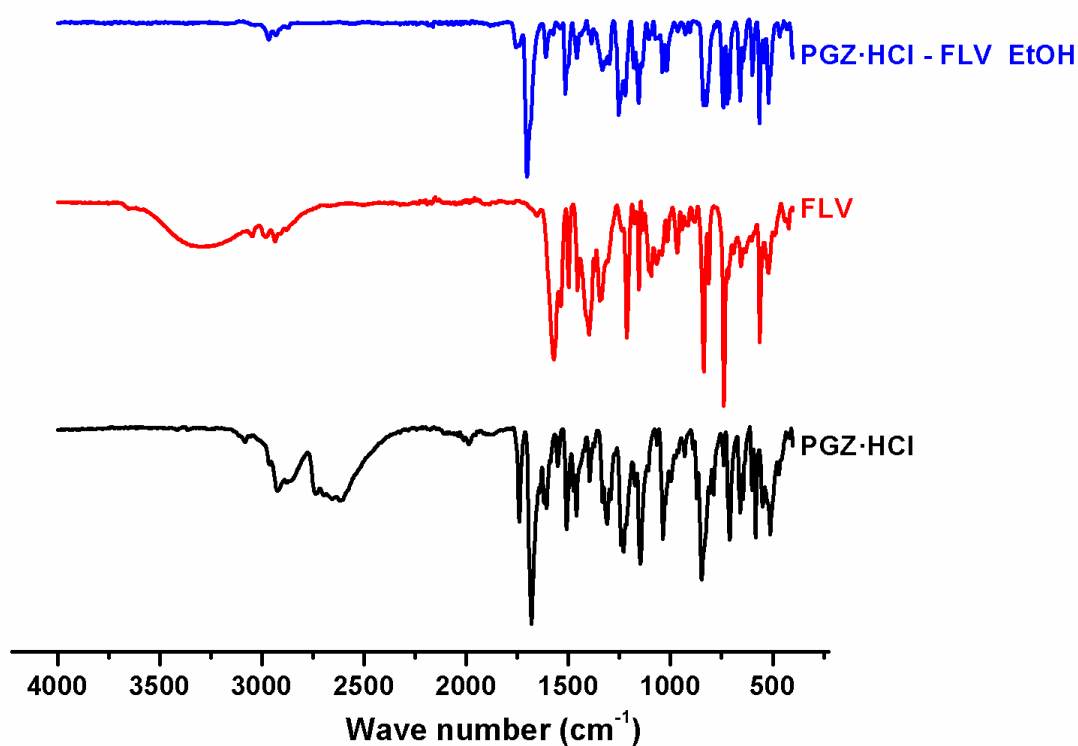
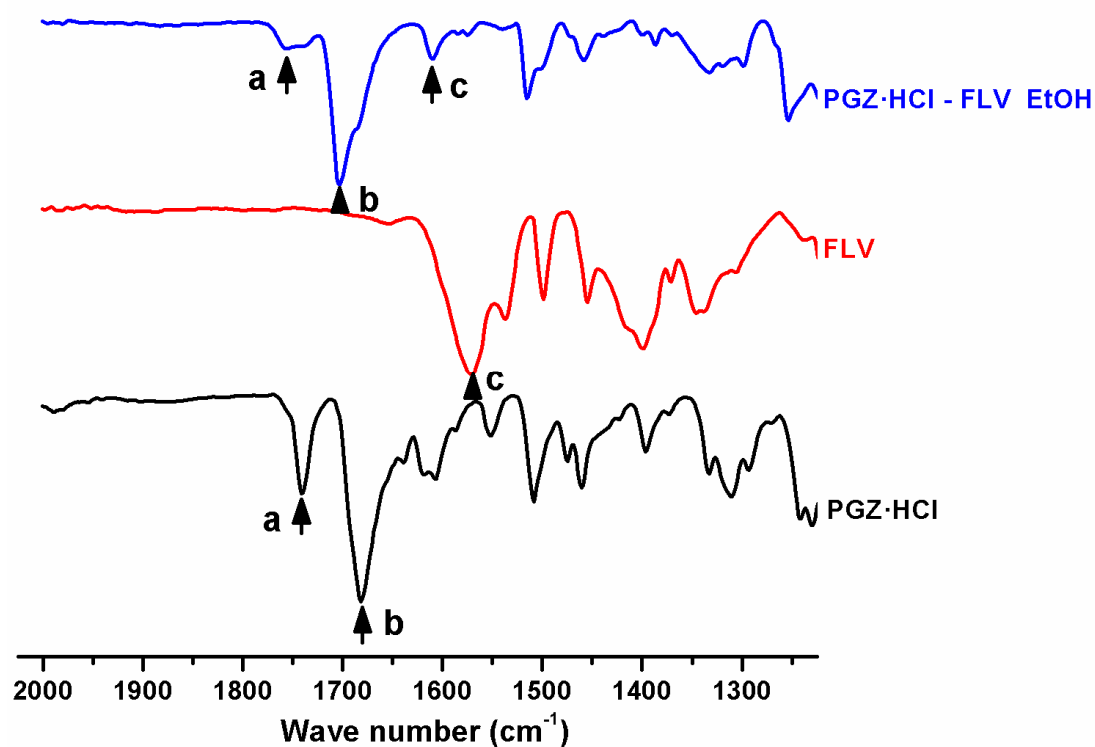


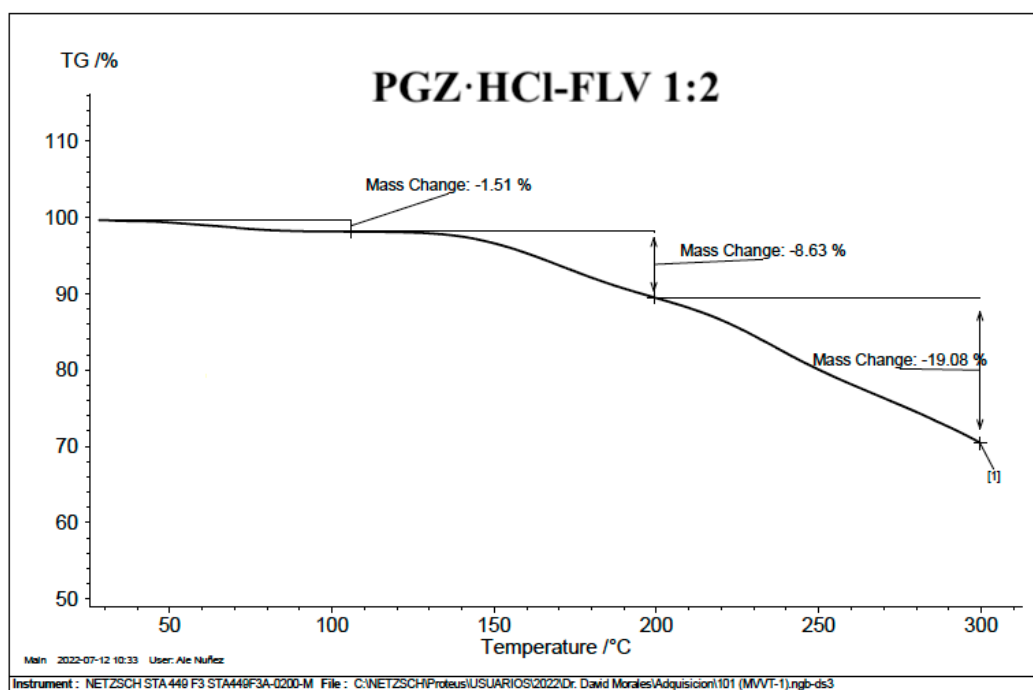
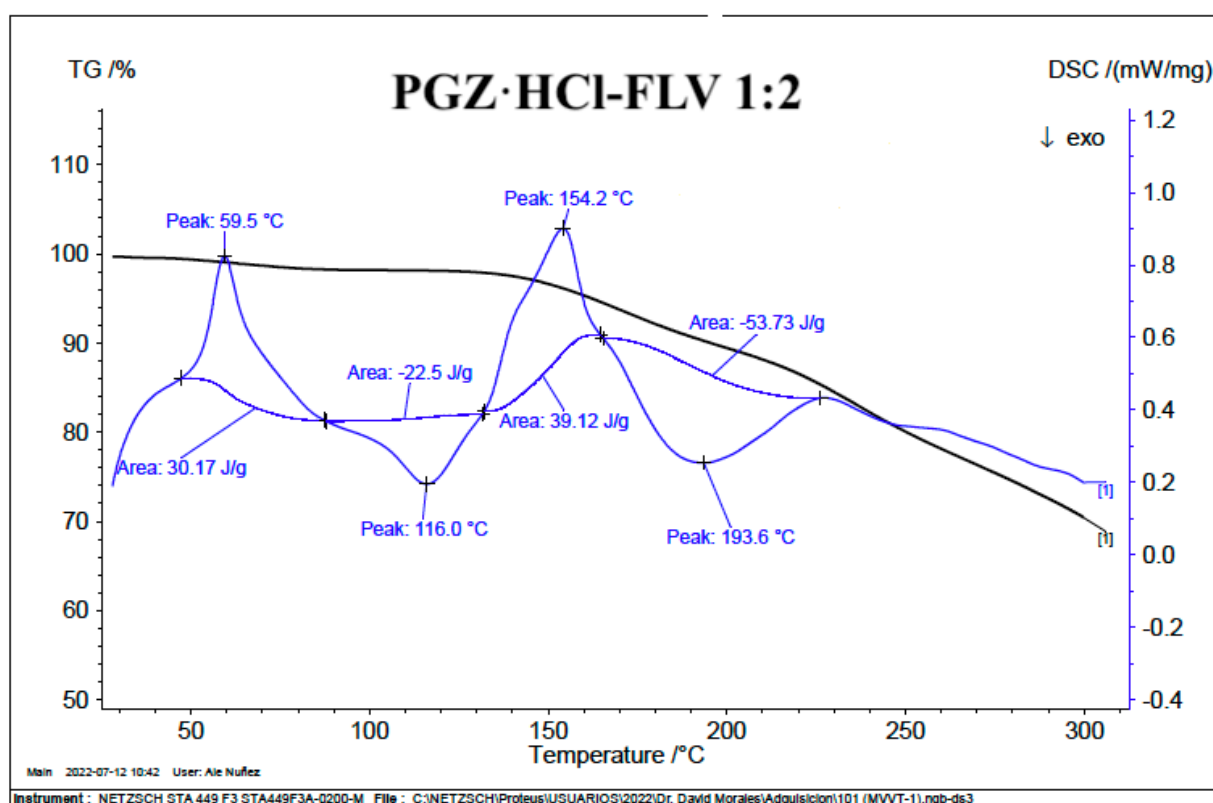
Figure SM5. XPS spectra of PGZHCl, FLV and the binary solid form (EtOH)

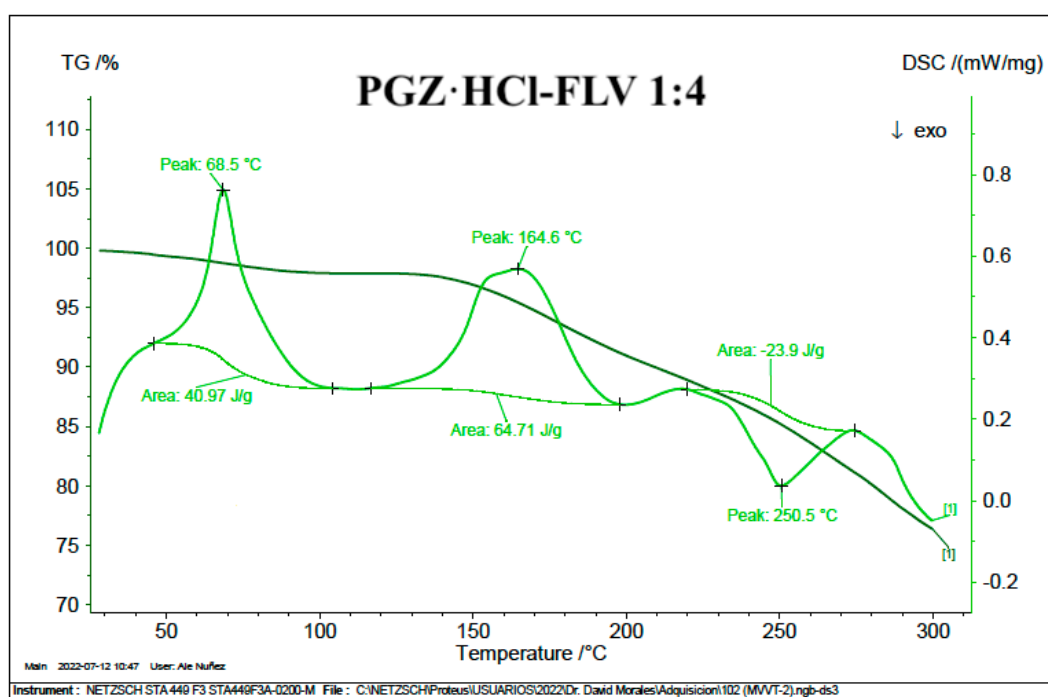
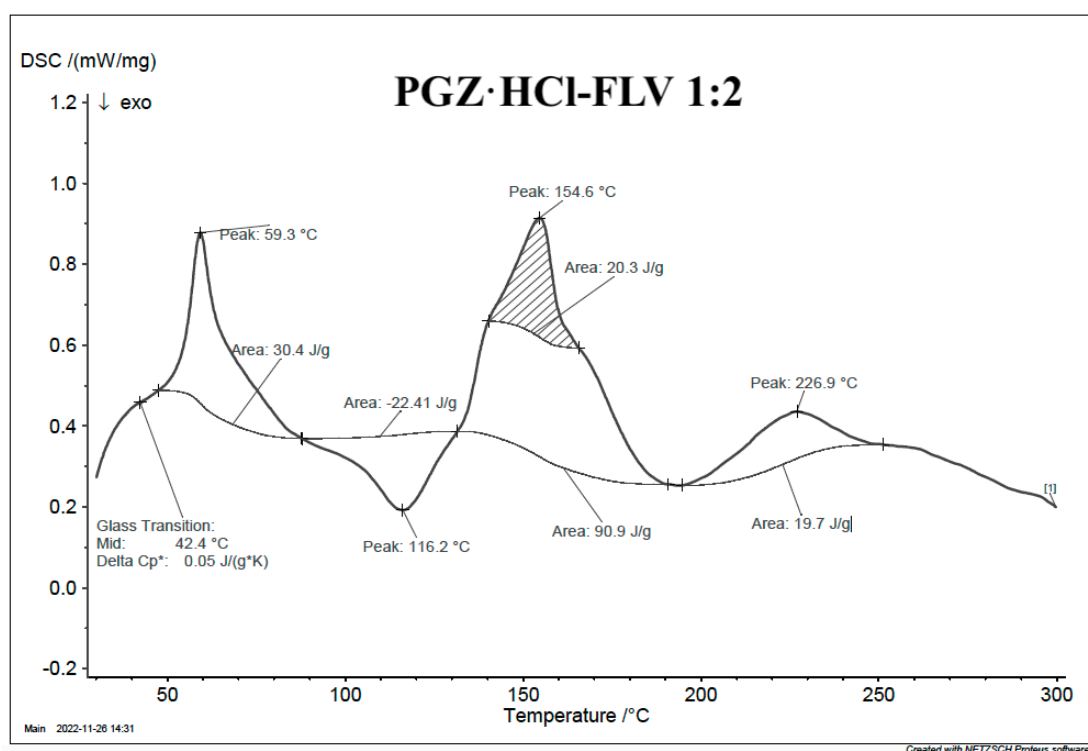


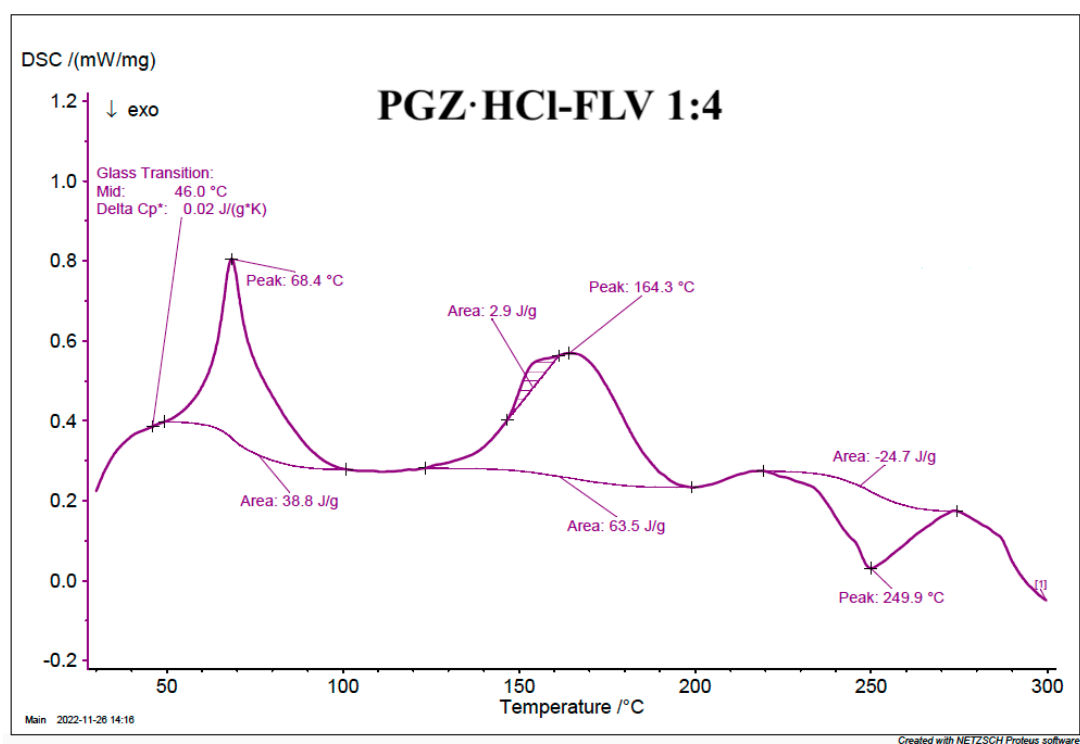
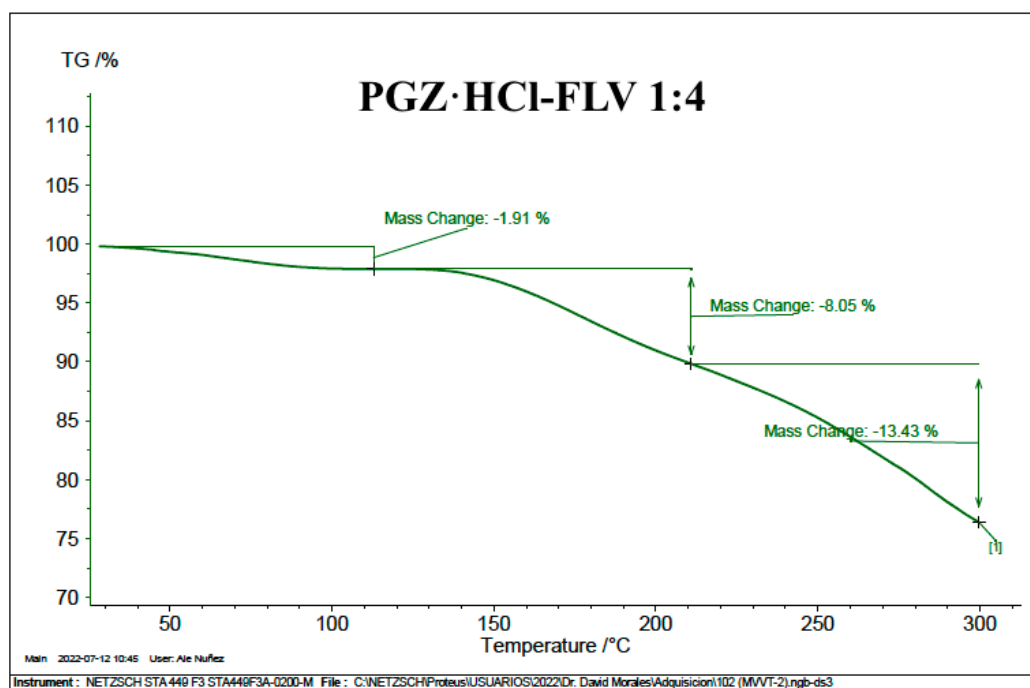


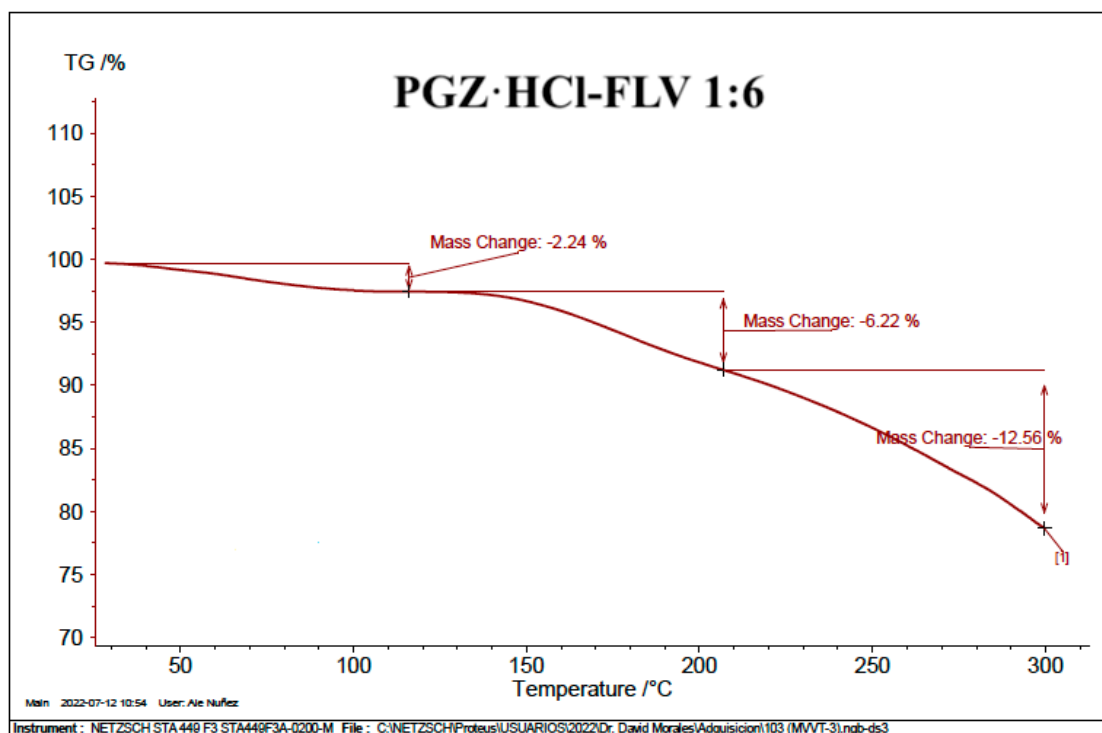
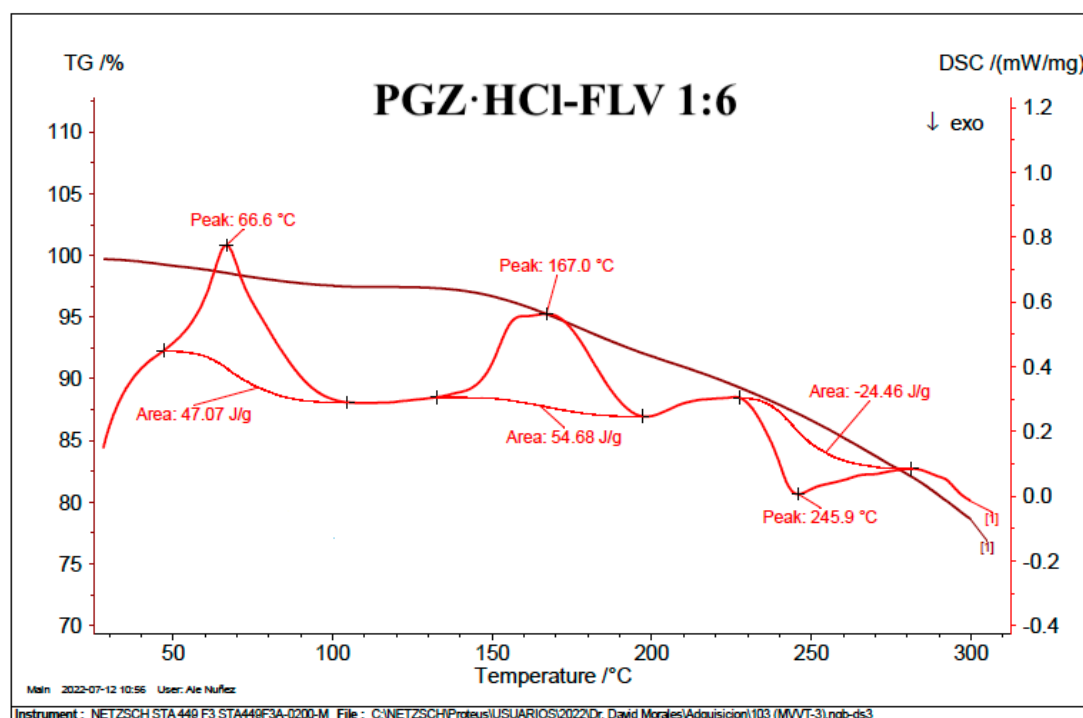
Vibrational band assignment	PGZ·HCl	FLV	PGZ·HCl-FLV (EtOH)
-C=O _{PGZ} (a,b) ($\Delta\nu$ cm ⁻¹)	a: 1738 b: 1681		a: 1756 (18) b: 1702 (21)
-C=O _{FLV} (c) ($\Delta\nu$ cm ⁻¹)		c: 1571	c: 1610 (39)
$ \Delta\nu$ cm ⁻¹ = vibration mode of pure drug - vibration mode of solid binary form			

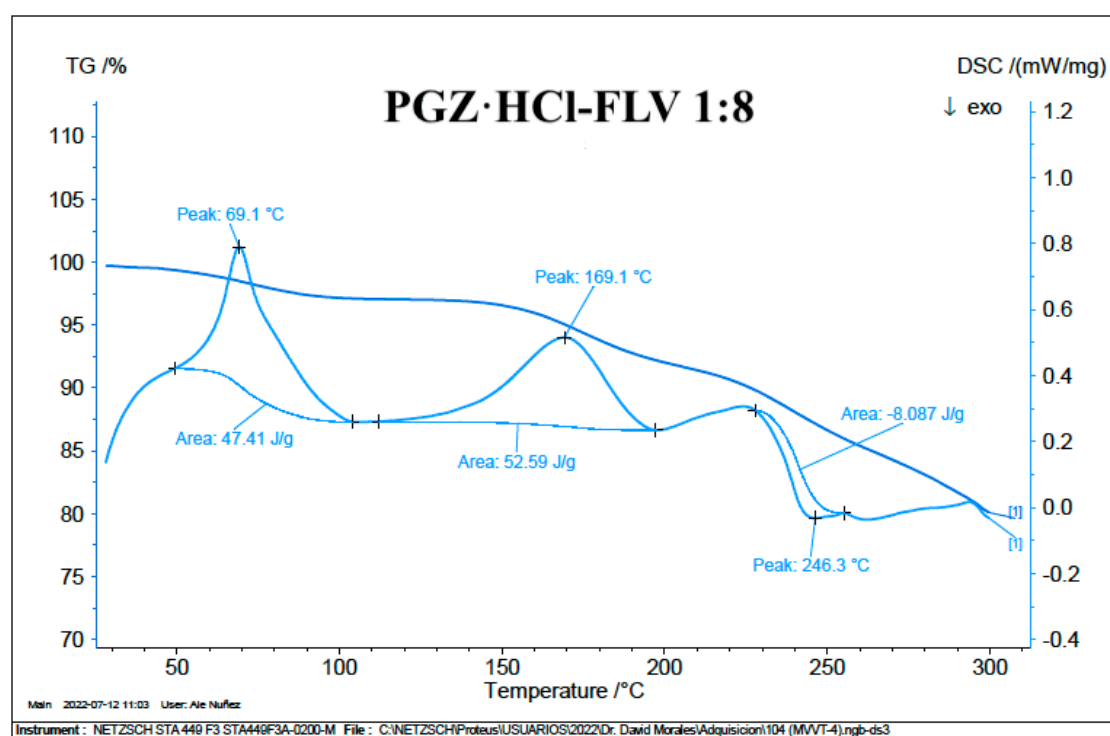
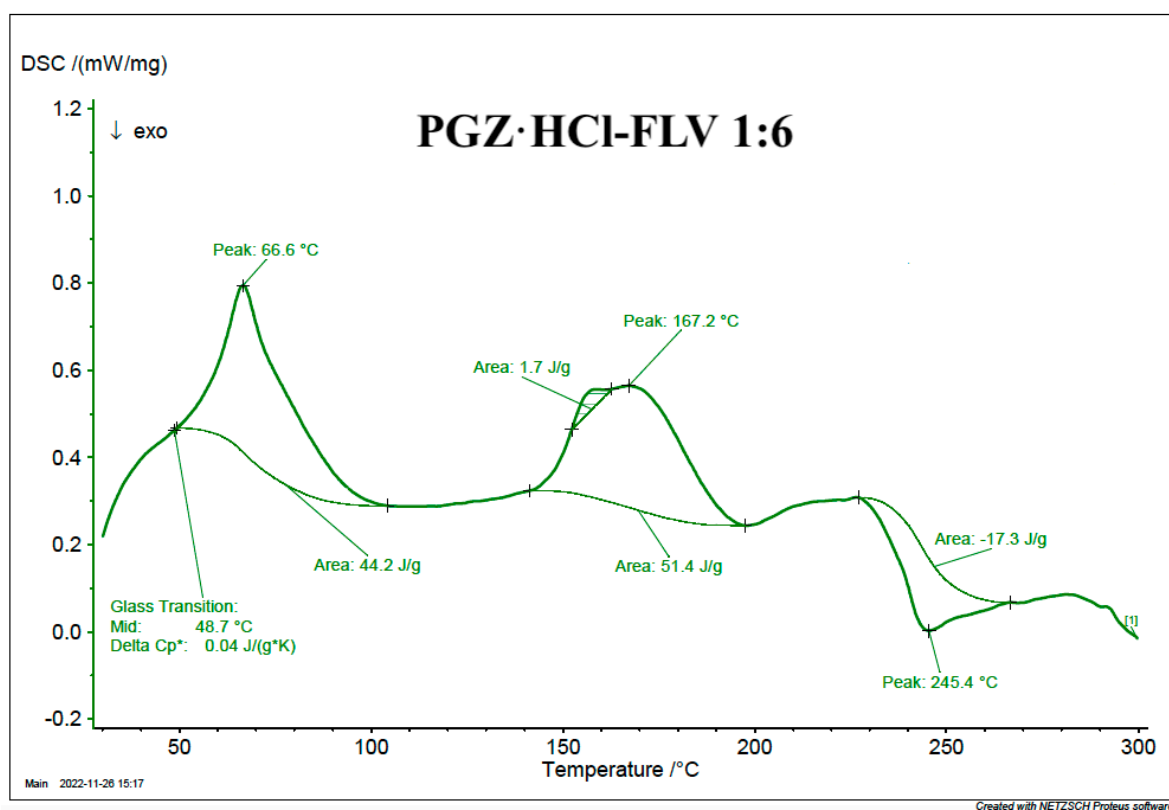
Figure SM6. Full and extended PGZHCl, FLV, and PGZ-FLV (EtOH) FTIR spectra. Likewise, the table indicates the frequency values.

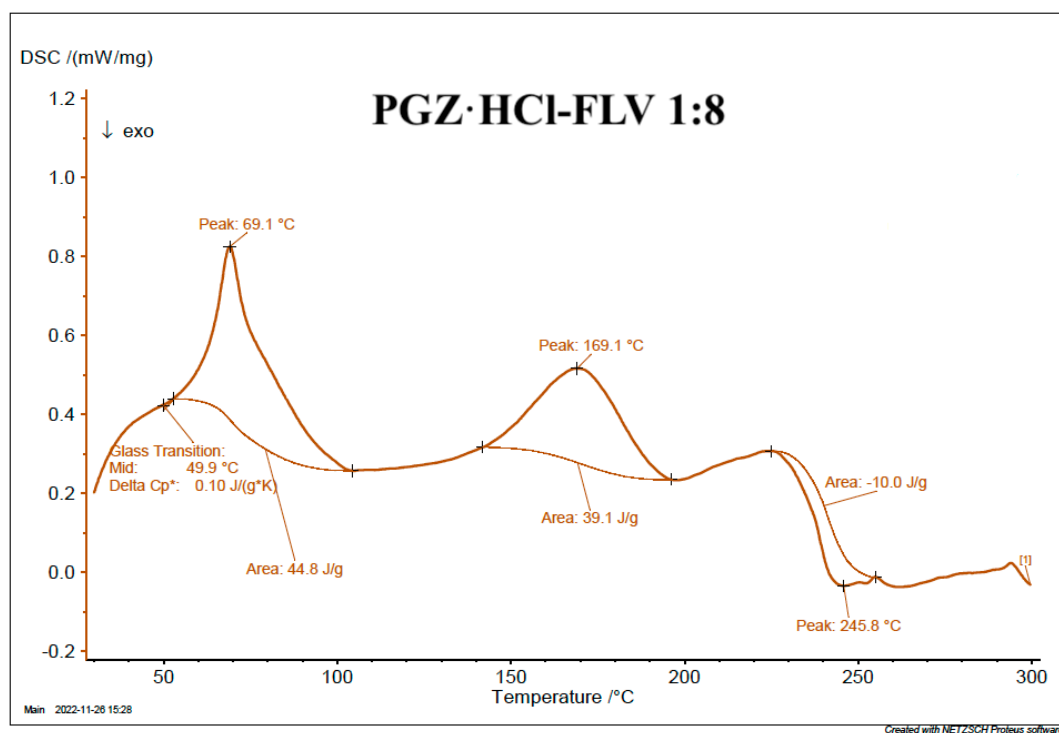
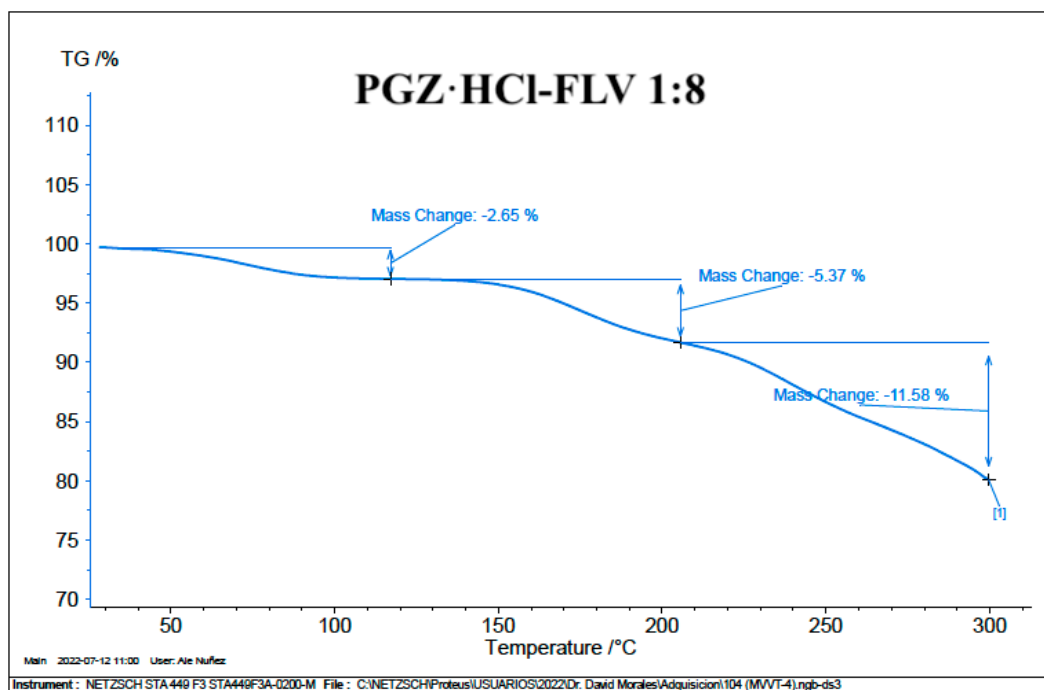


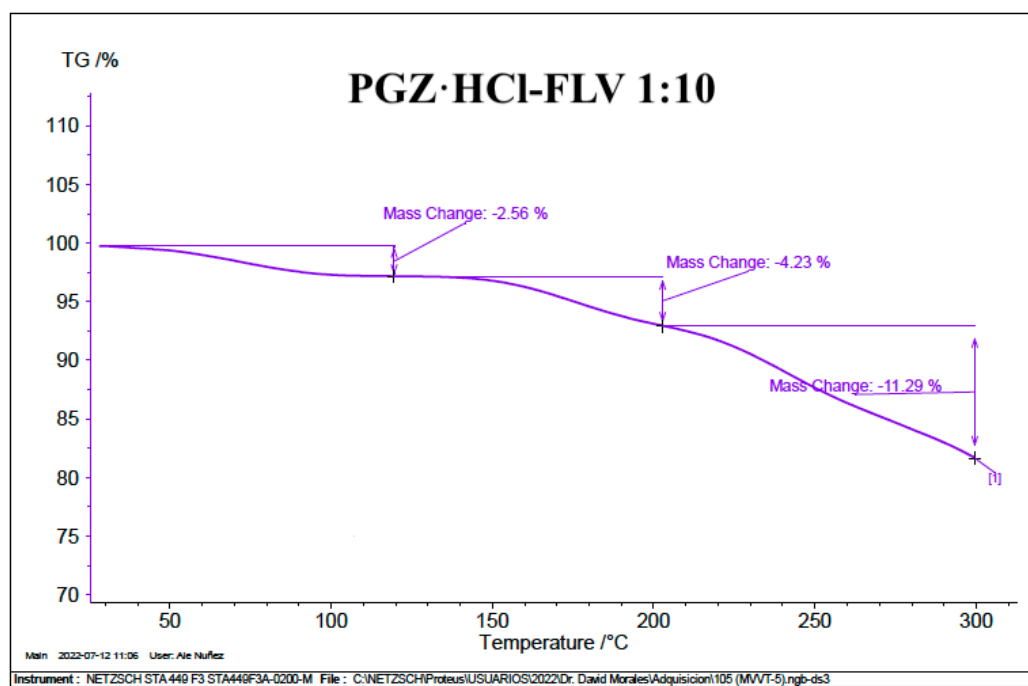
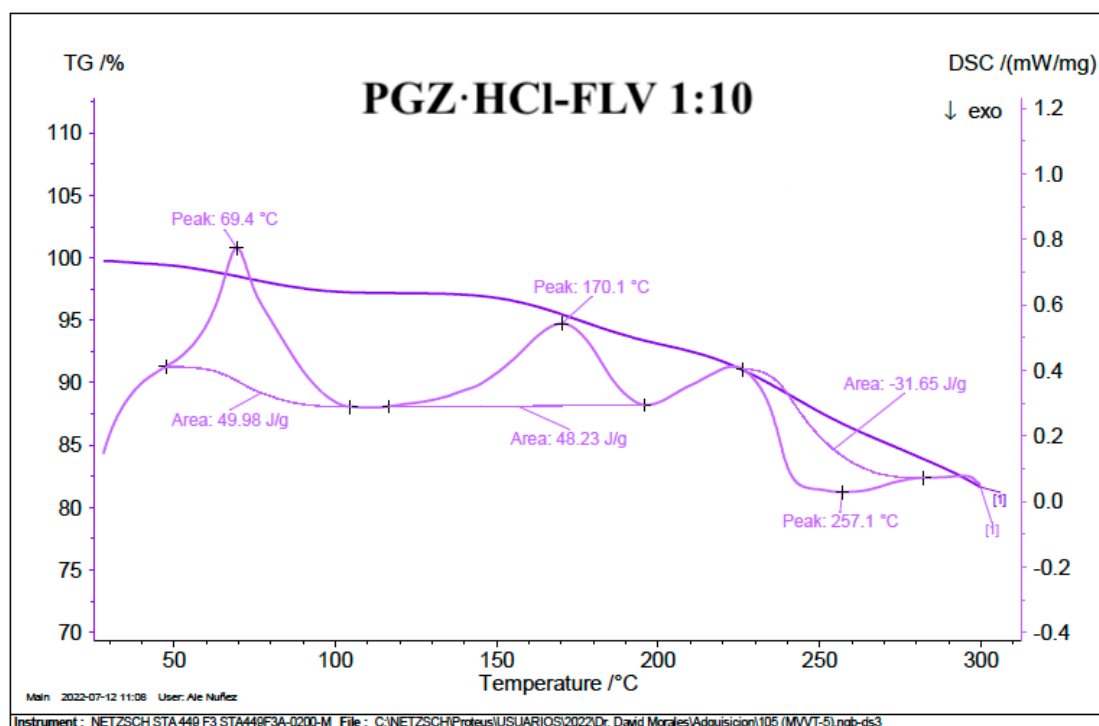












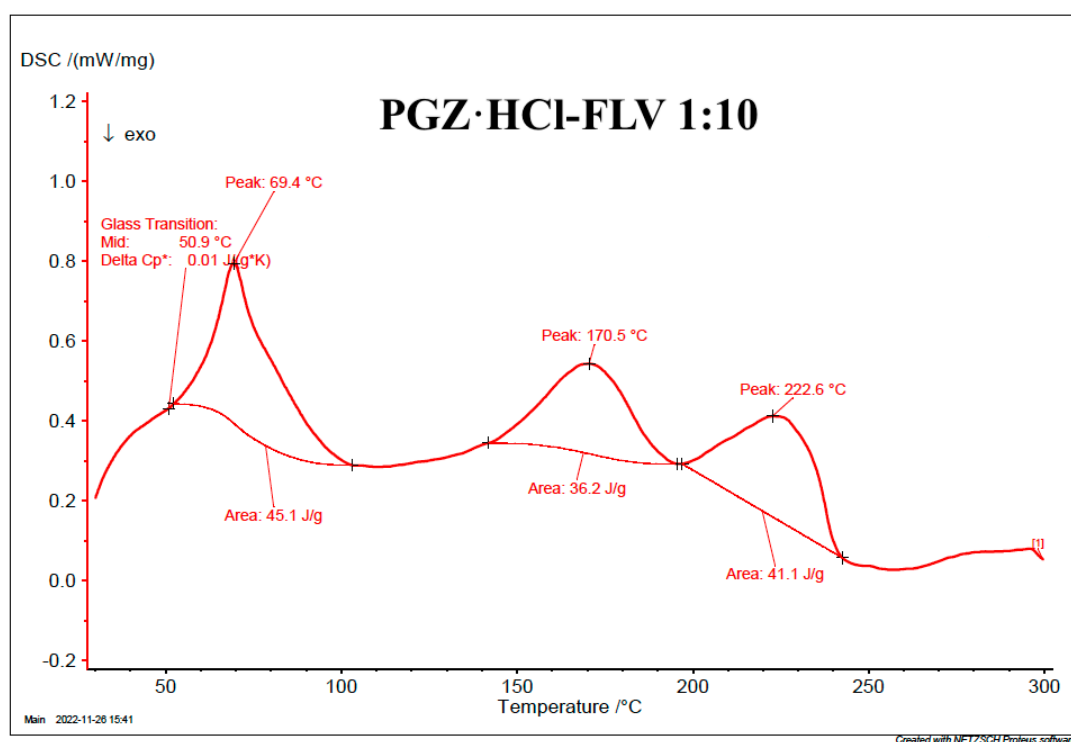


Figure SM7. Individual DSC-TGA thermograms of the solid forms of PGZ·HCl-FLV at different stoichiometric ratios (1:2; 1:4; 1:6; 1:8 and 1:10)

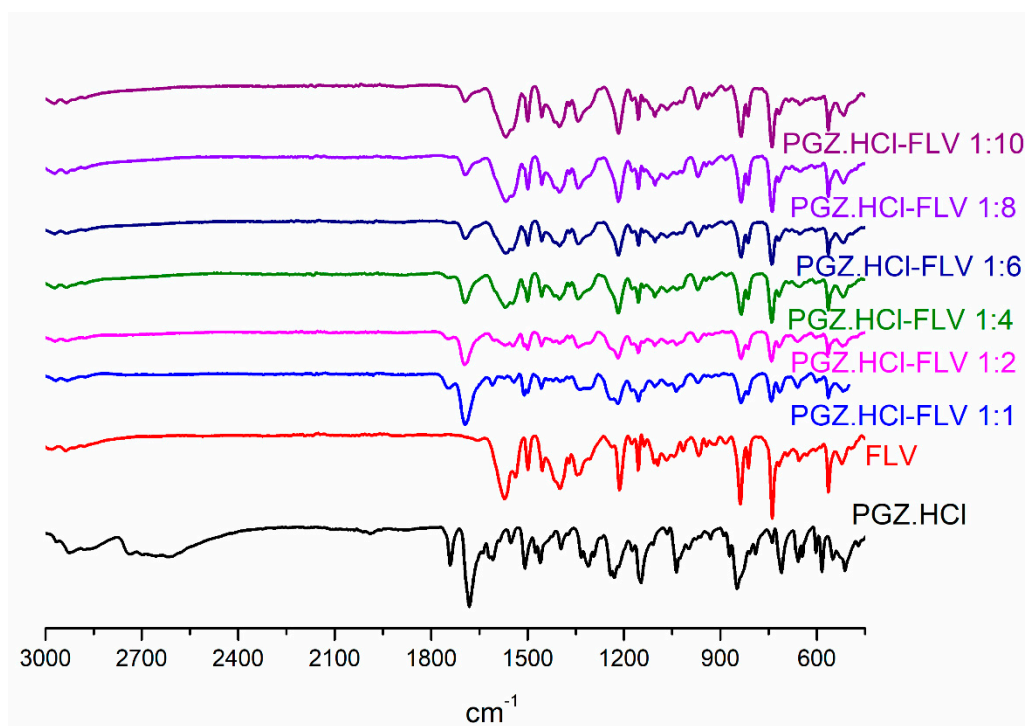
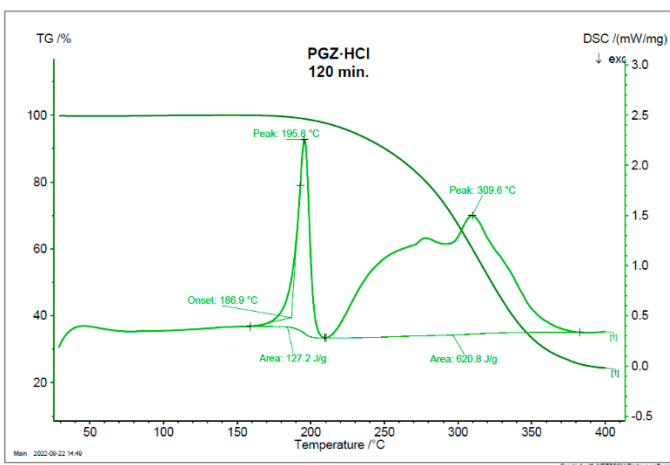
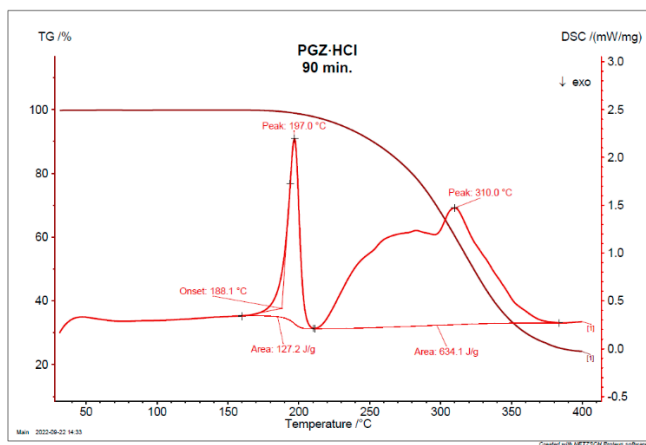
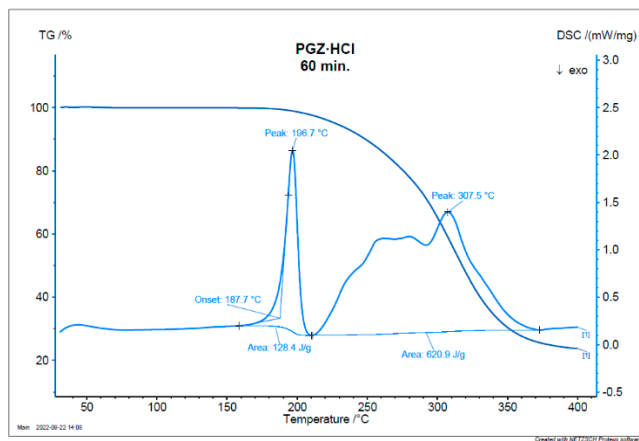
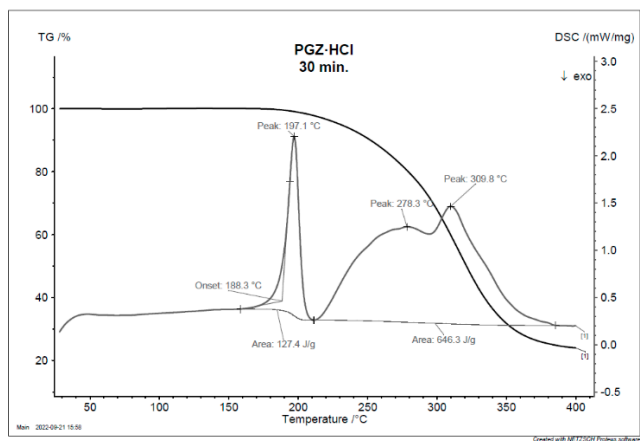
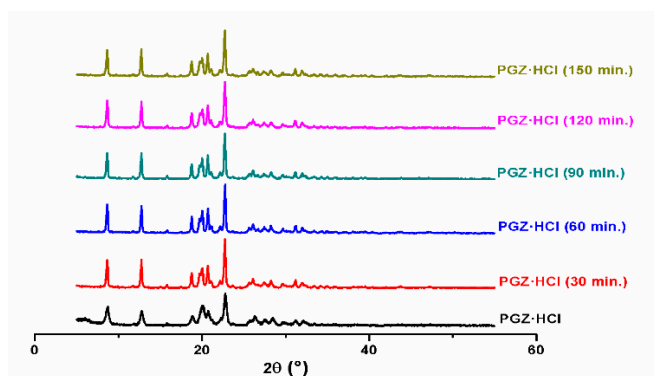
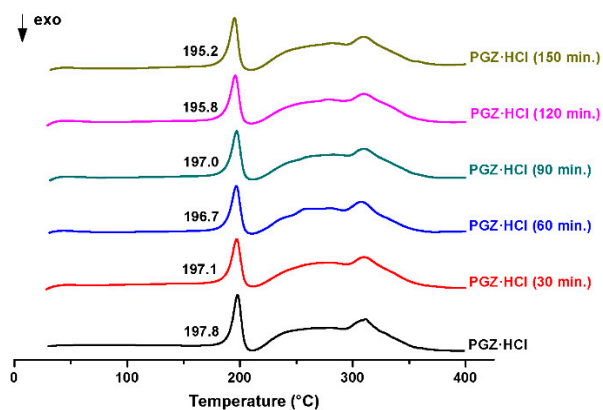


Figure SM8. Full FT-IR spectra of the solid forms of PGZ·HCl-FLV at different stoichiometric ratios (1:1; 1:2; 1:4; 1:6; 1:8 and 1:10)



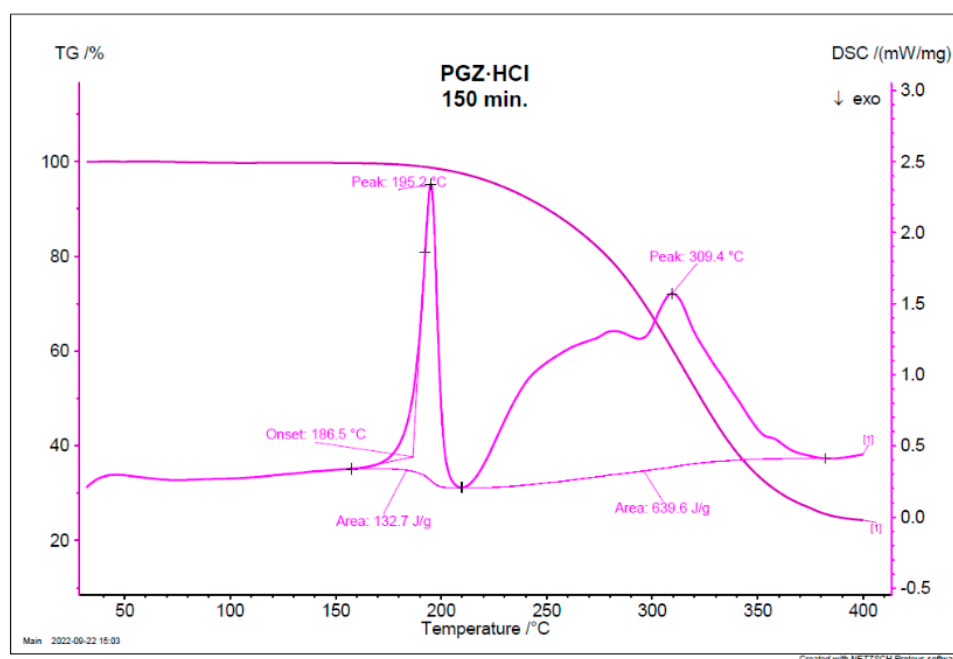
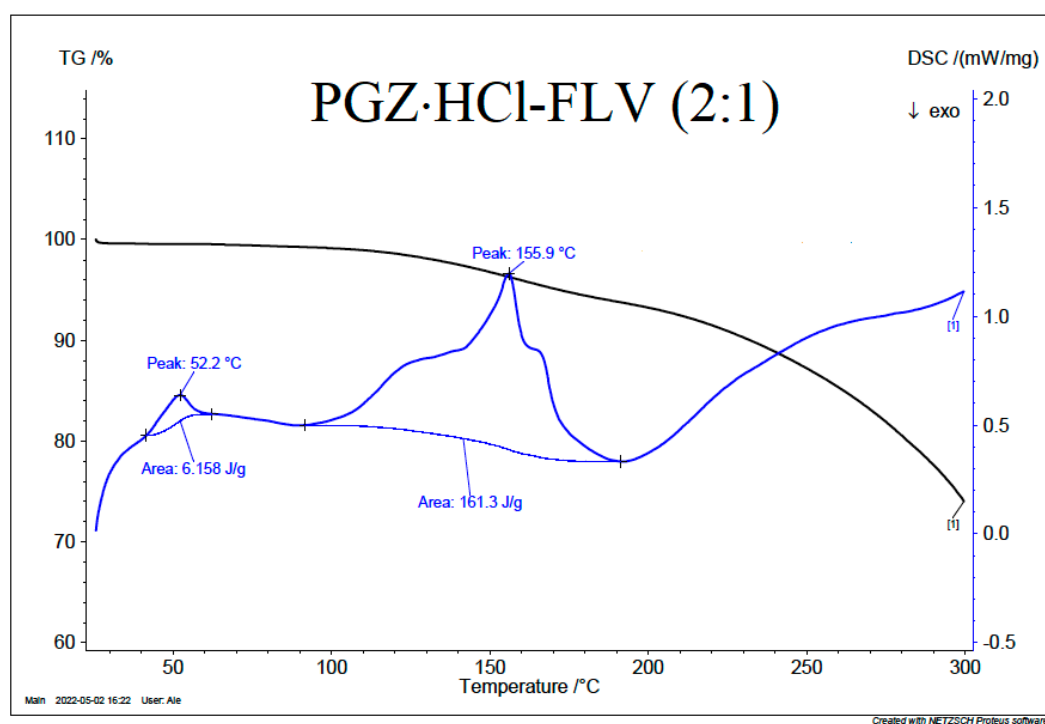
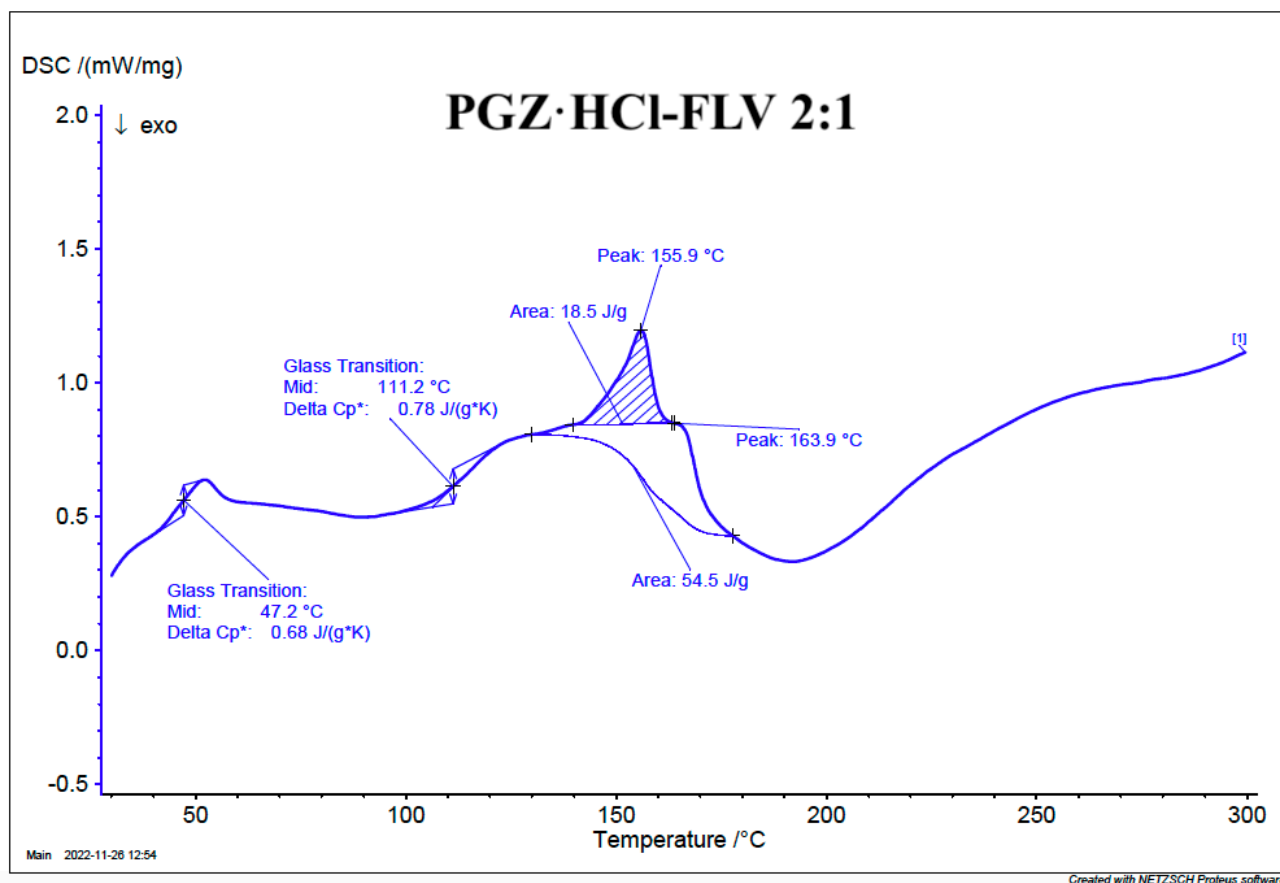
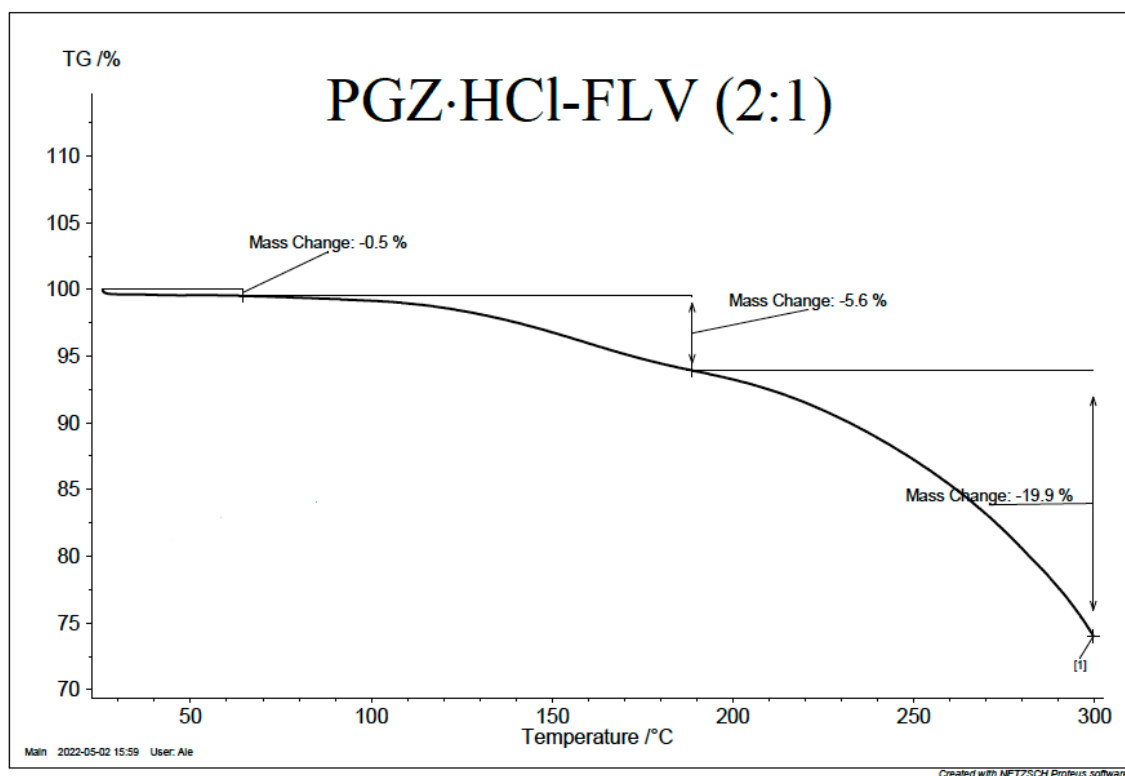
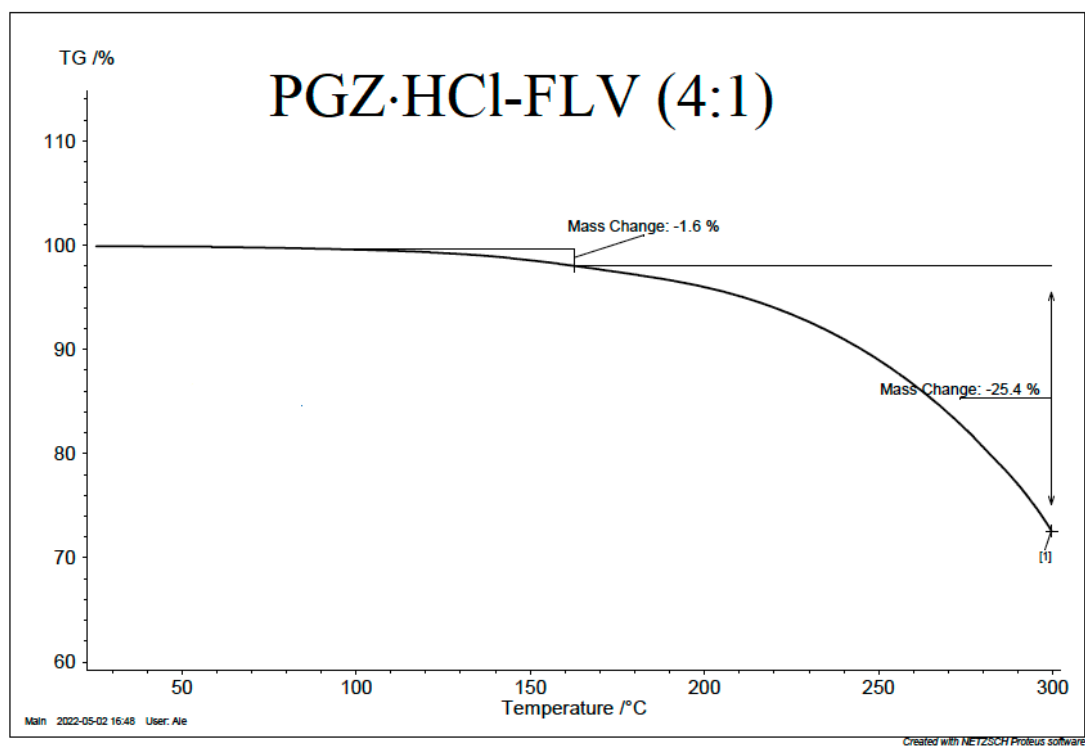
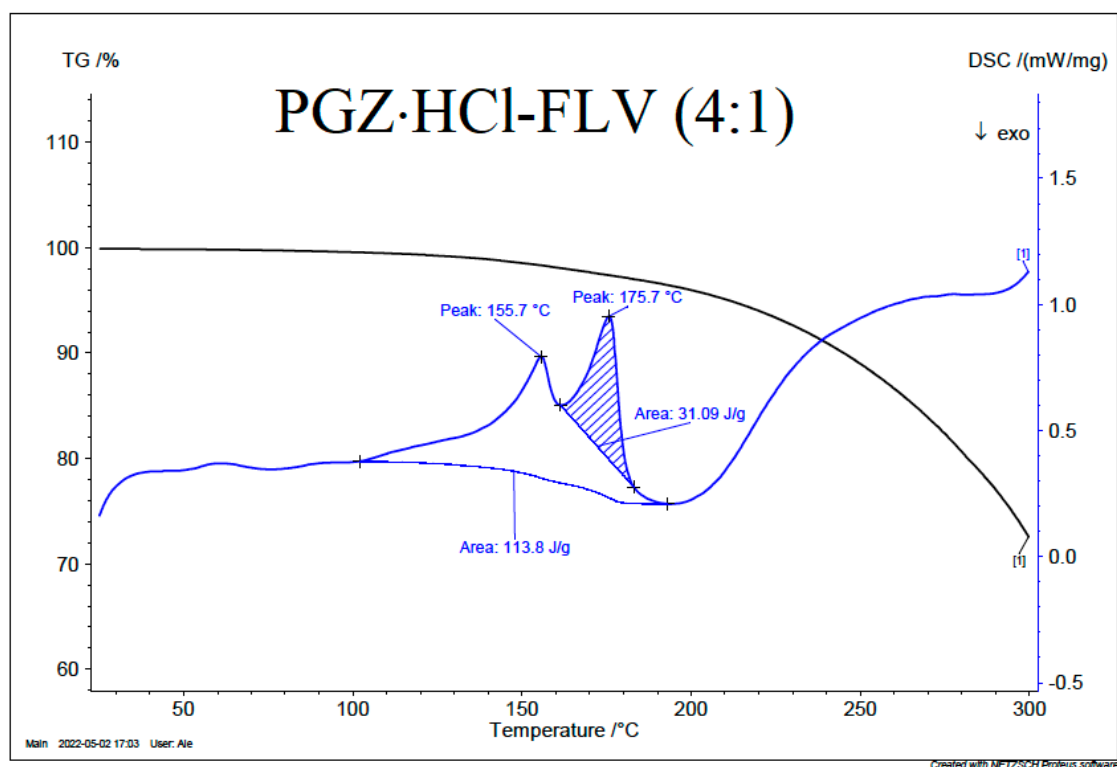
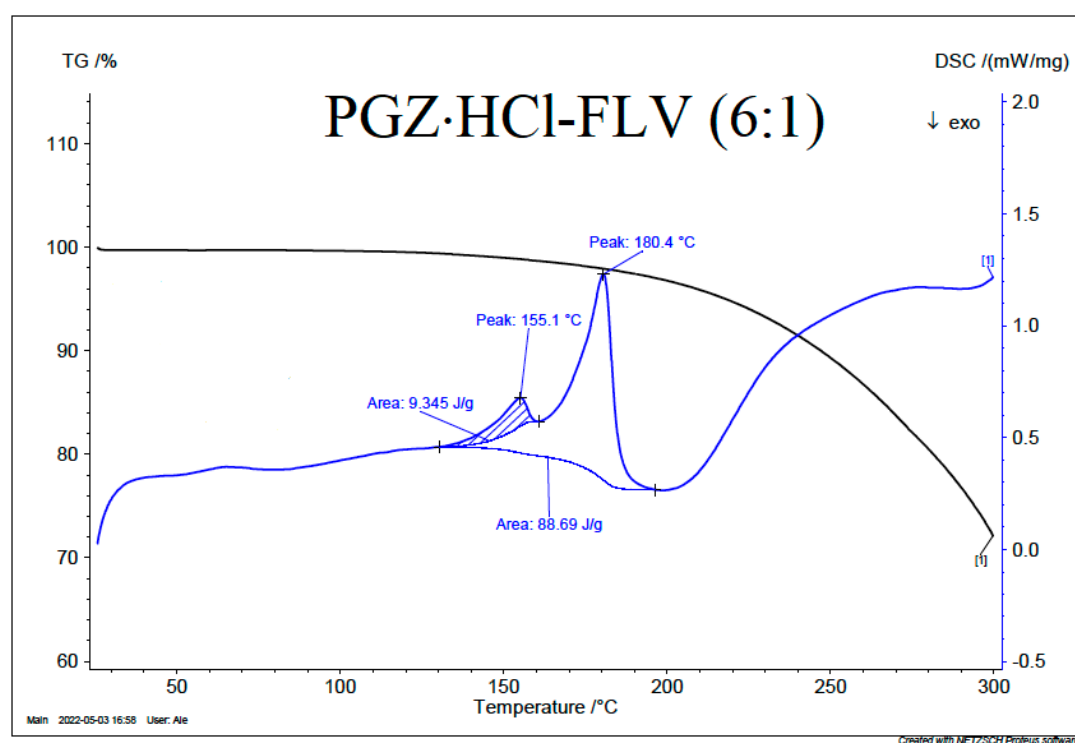
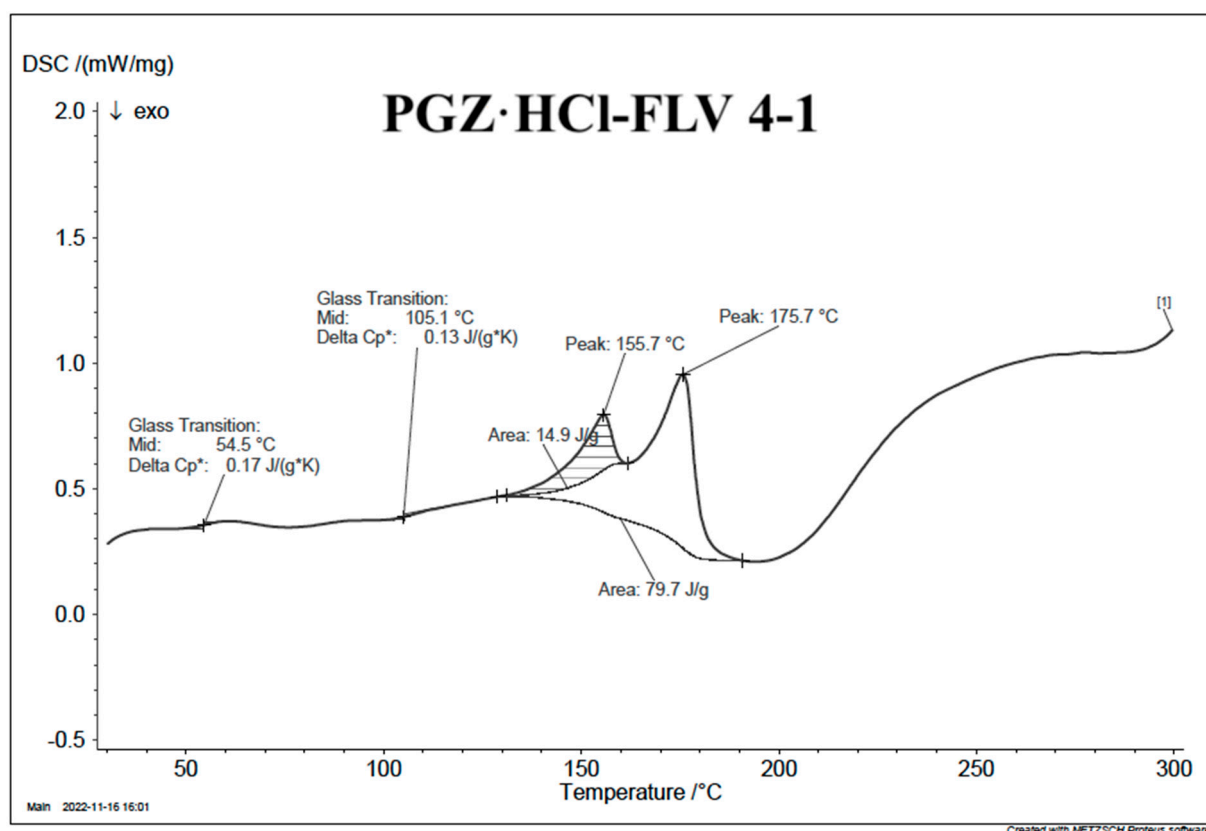


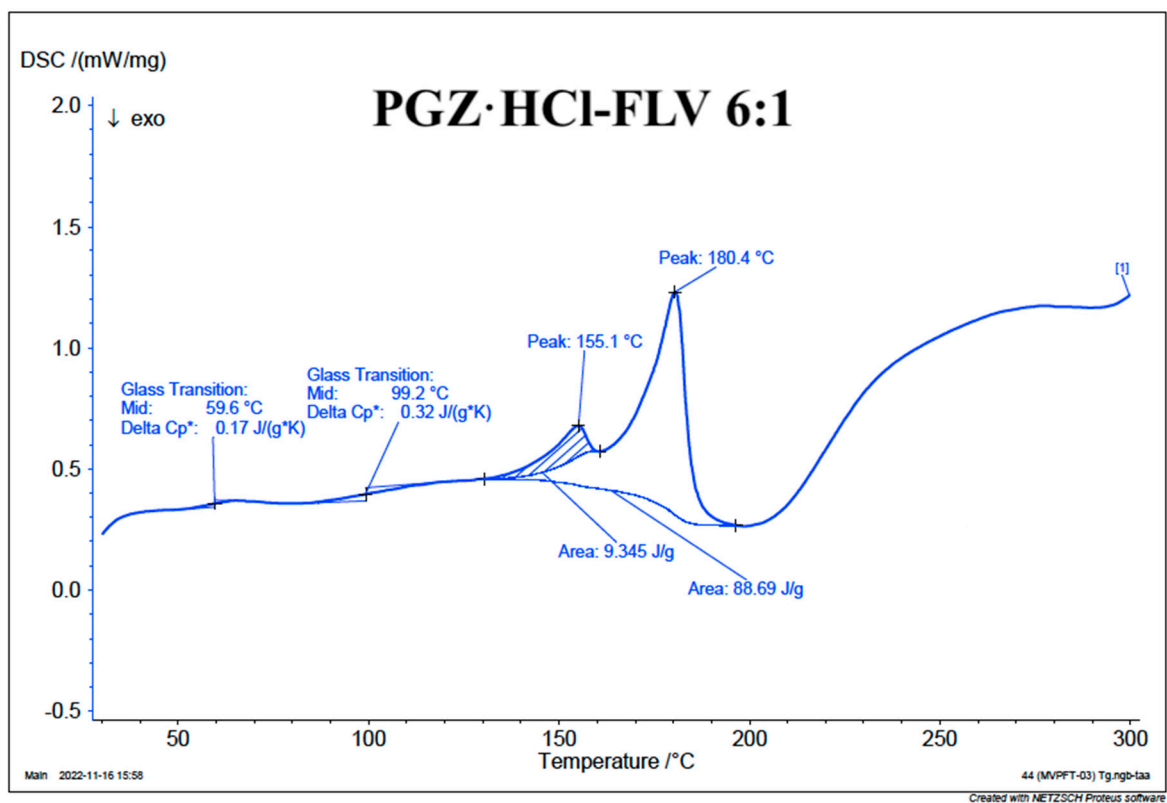
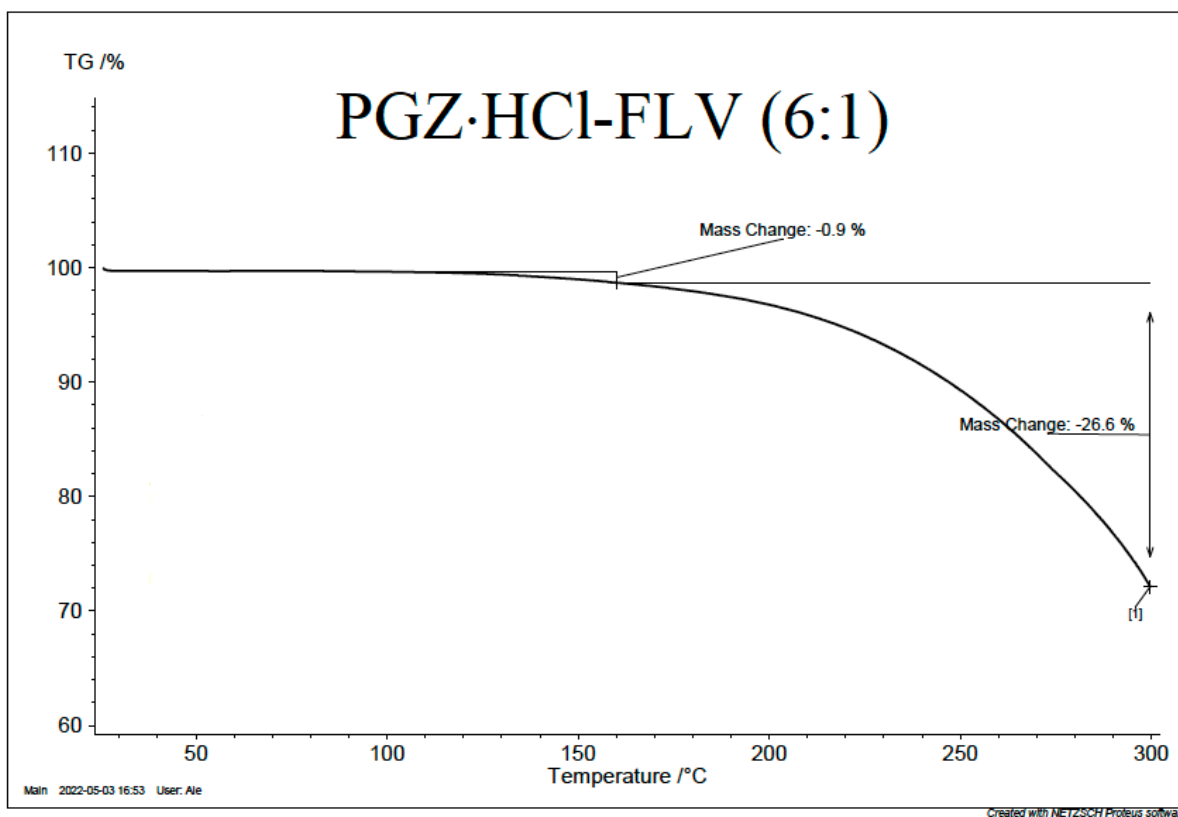
Figure SM9. Evaluation of the amorphization ability of the PGZ·HCl

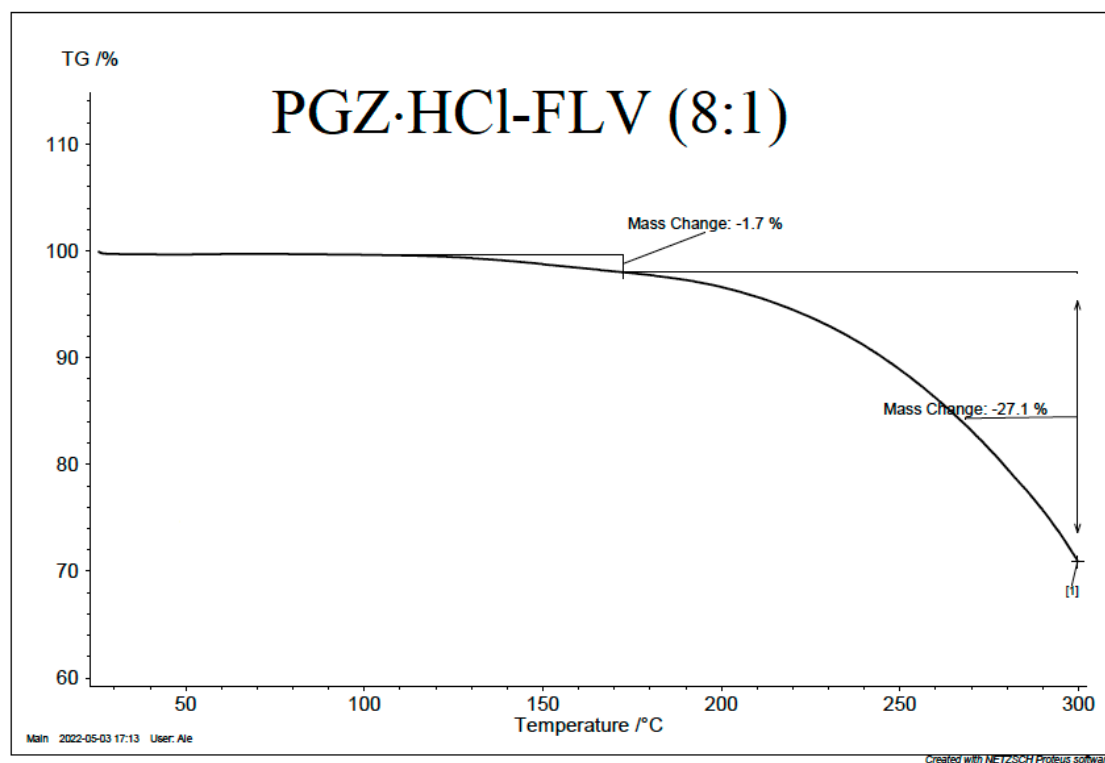
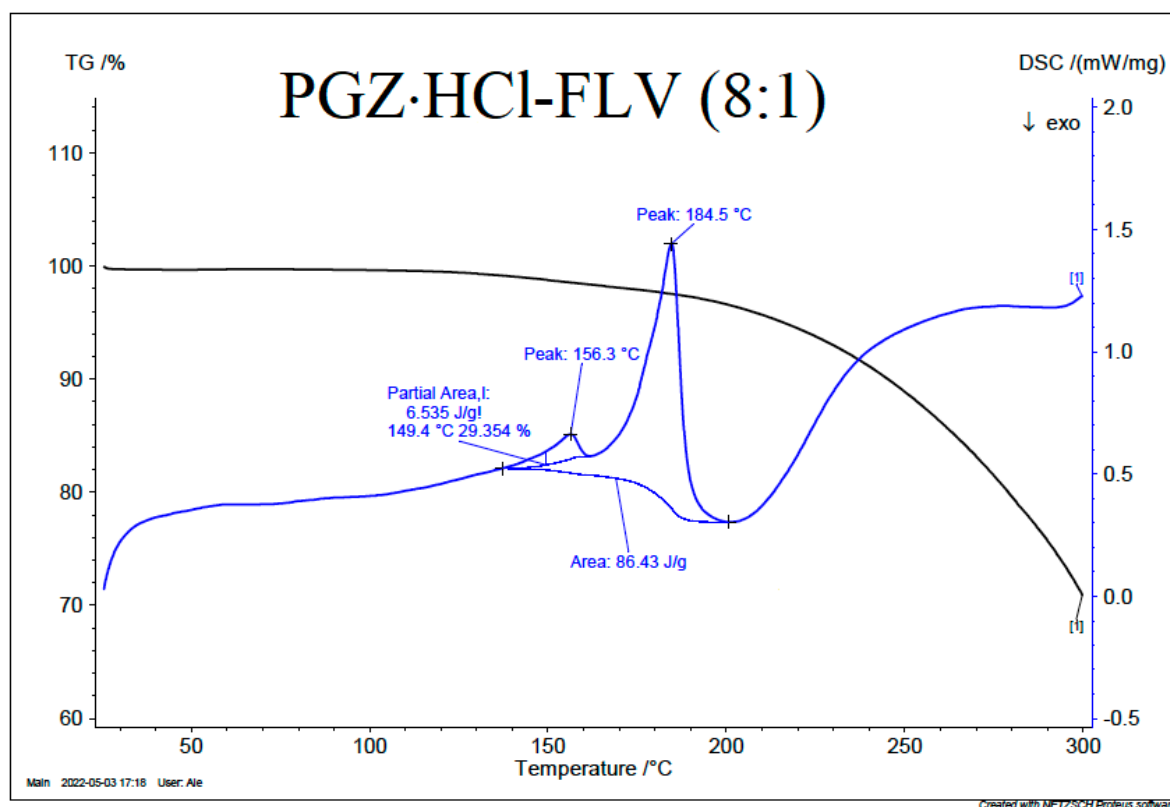


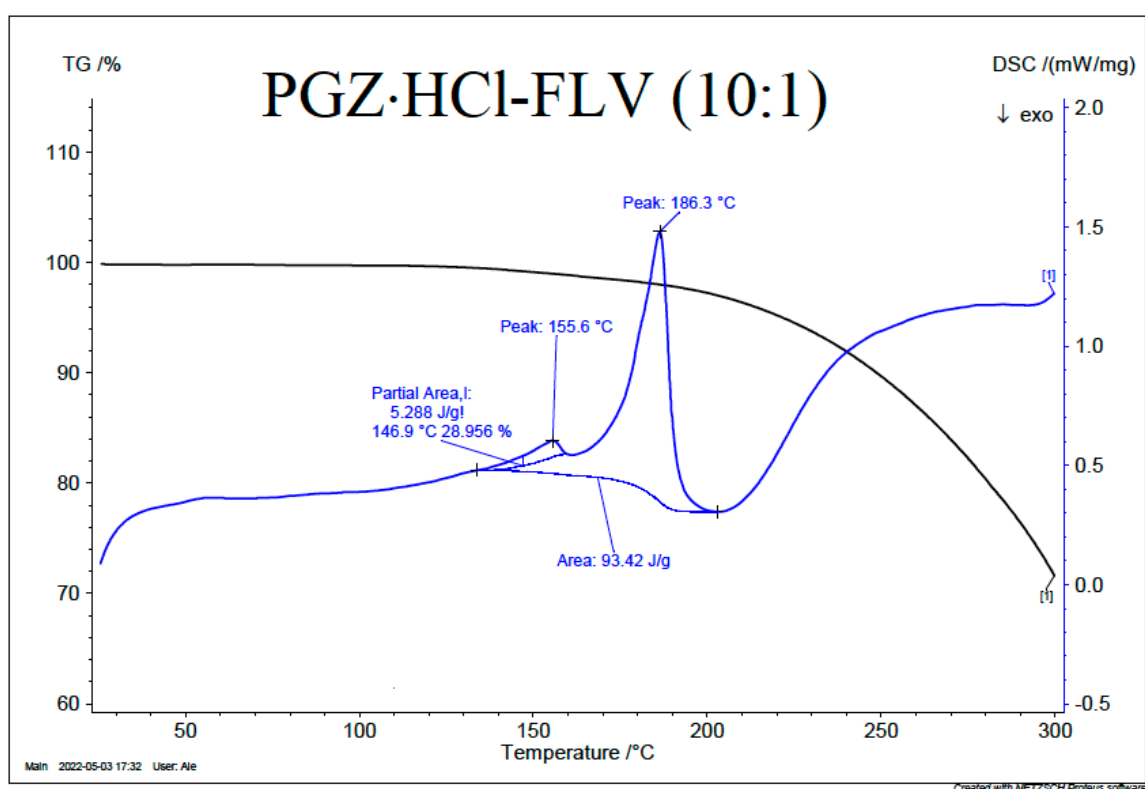
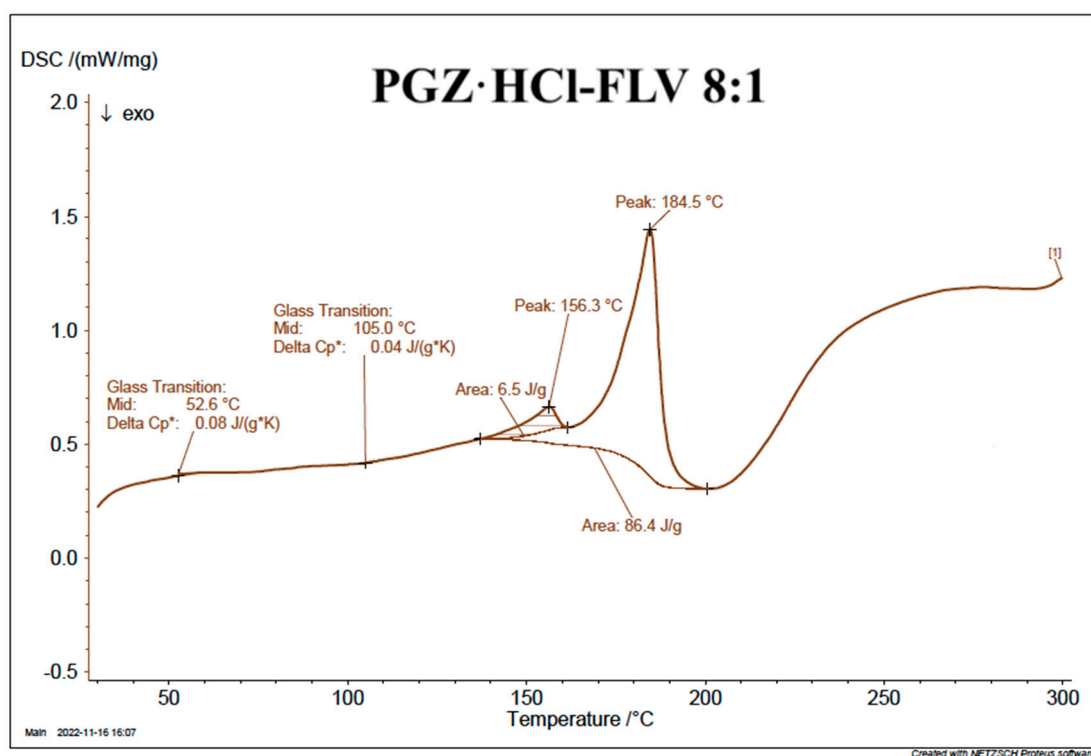












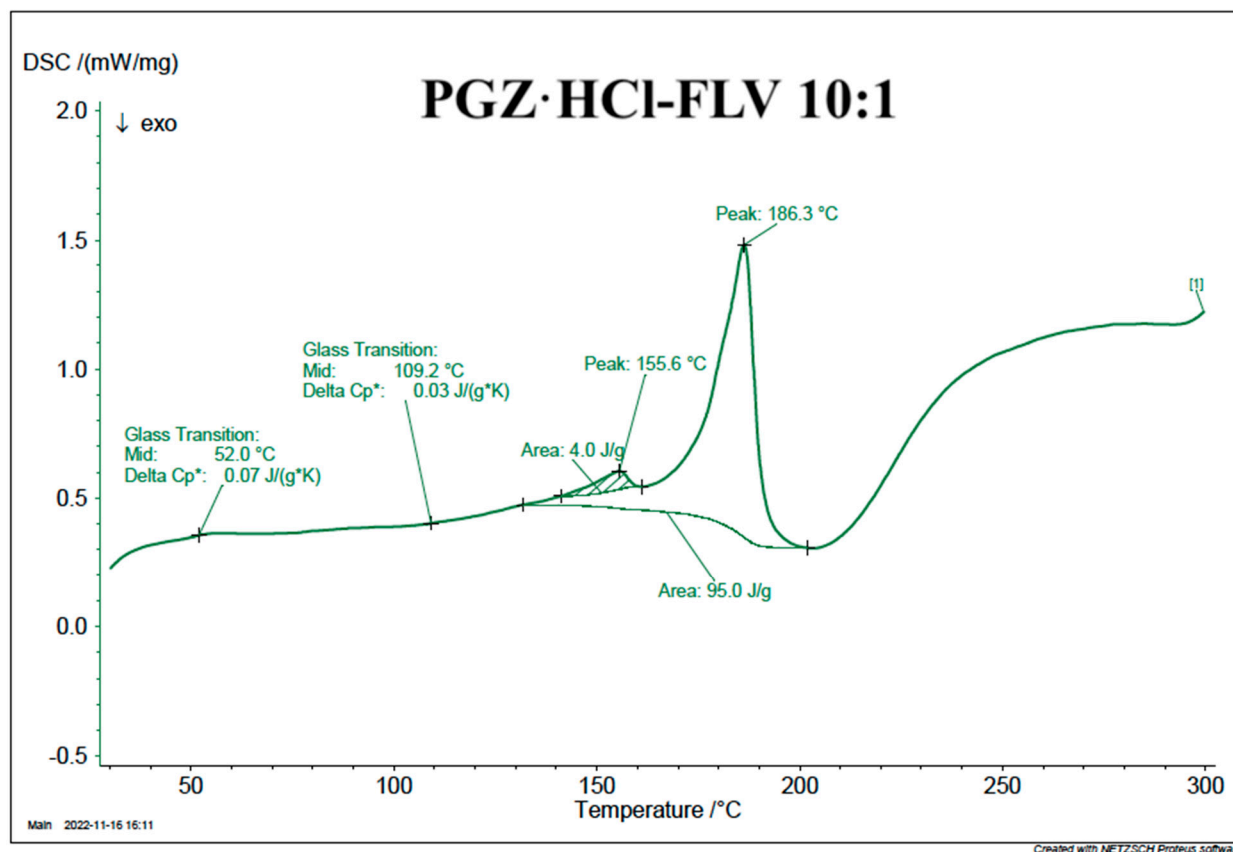
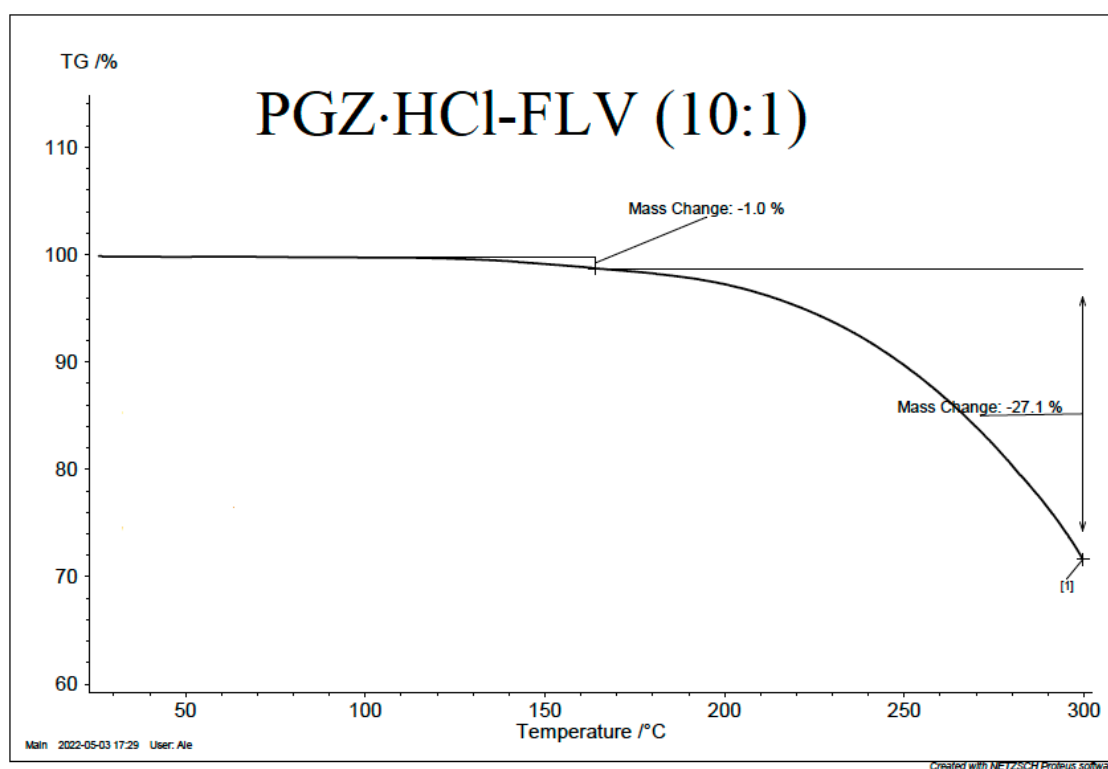


Figure SM10. Individual DSC-TGA thermograms of the solid forms of PGZ·HCl-FLV at different stoichiometric ratios (2:1; 4:1; 6:1; 8:1 and 10:1)

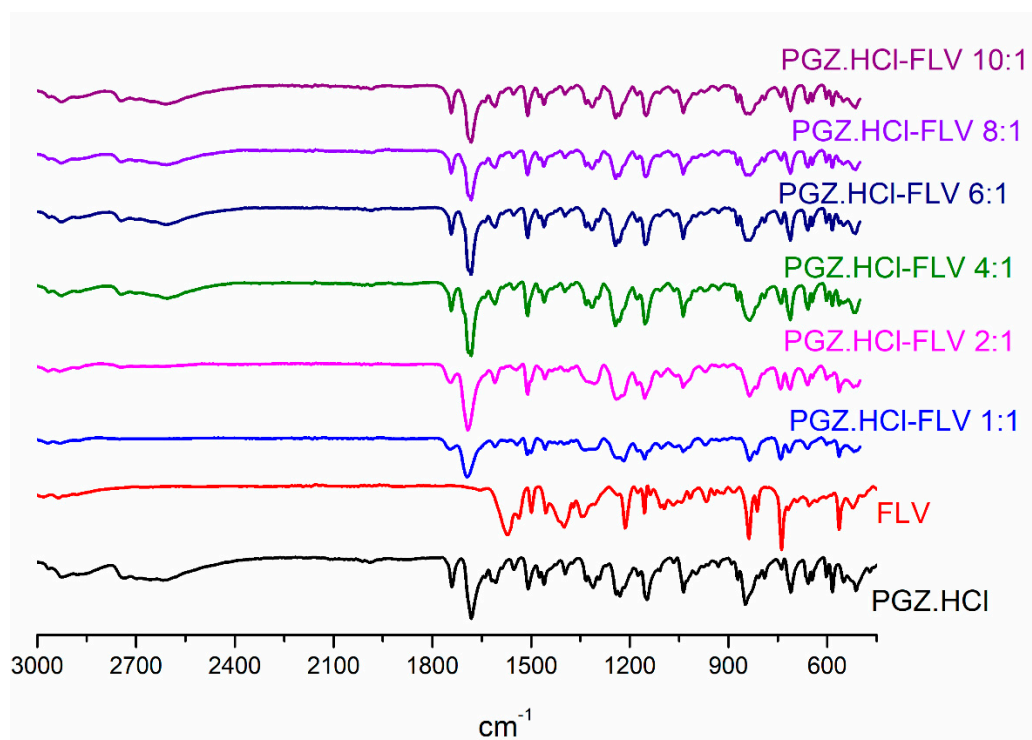
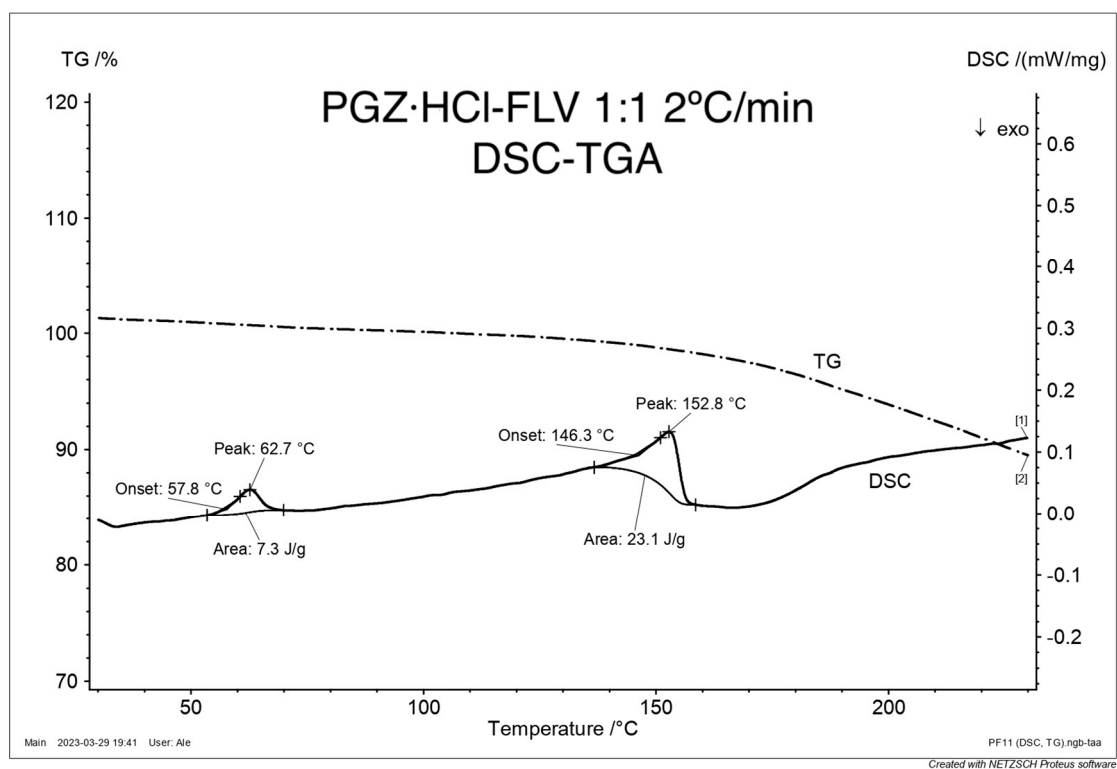
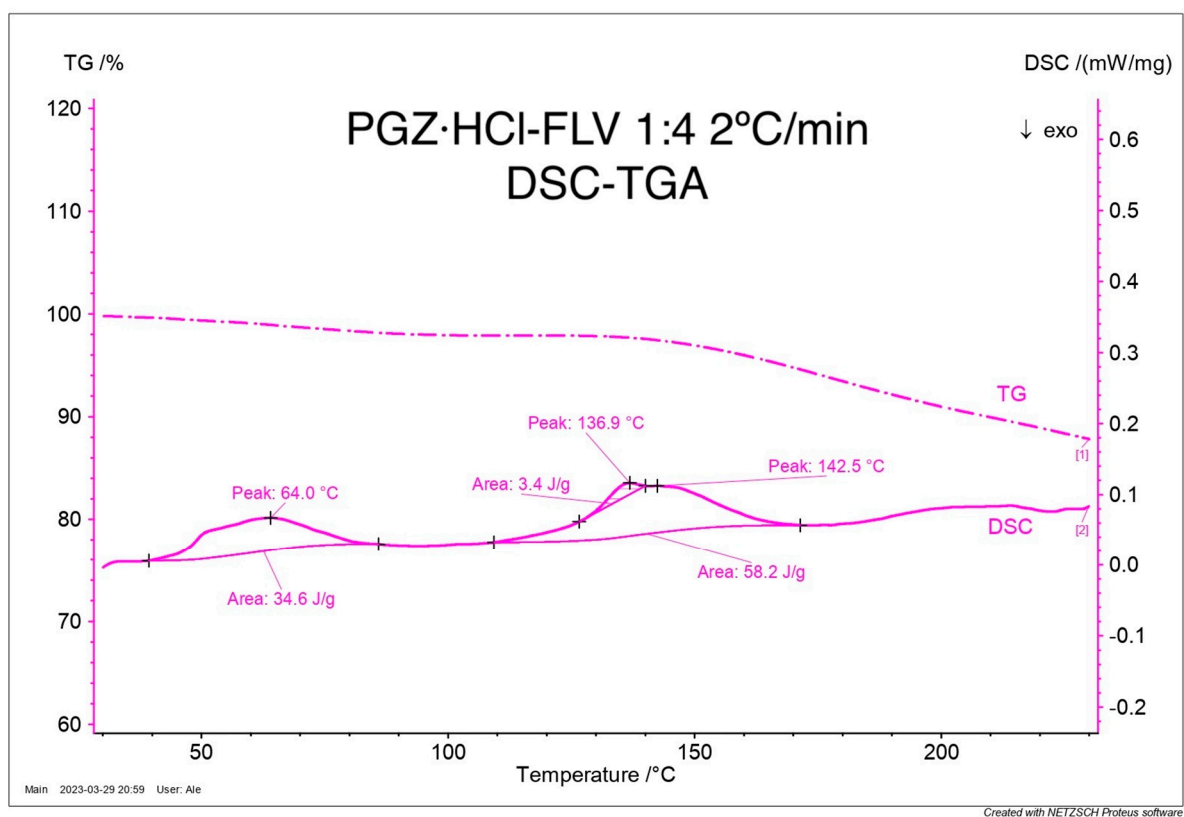
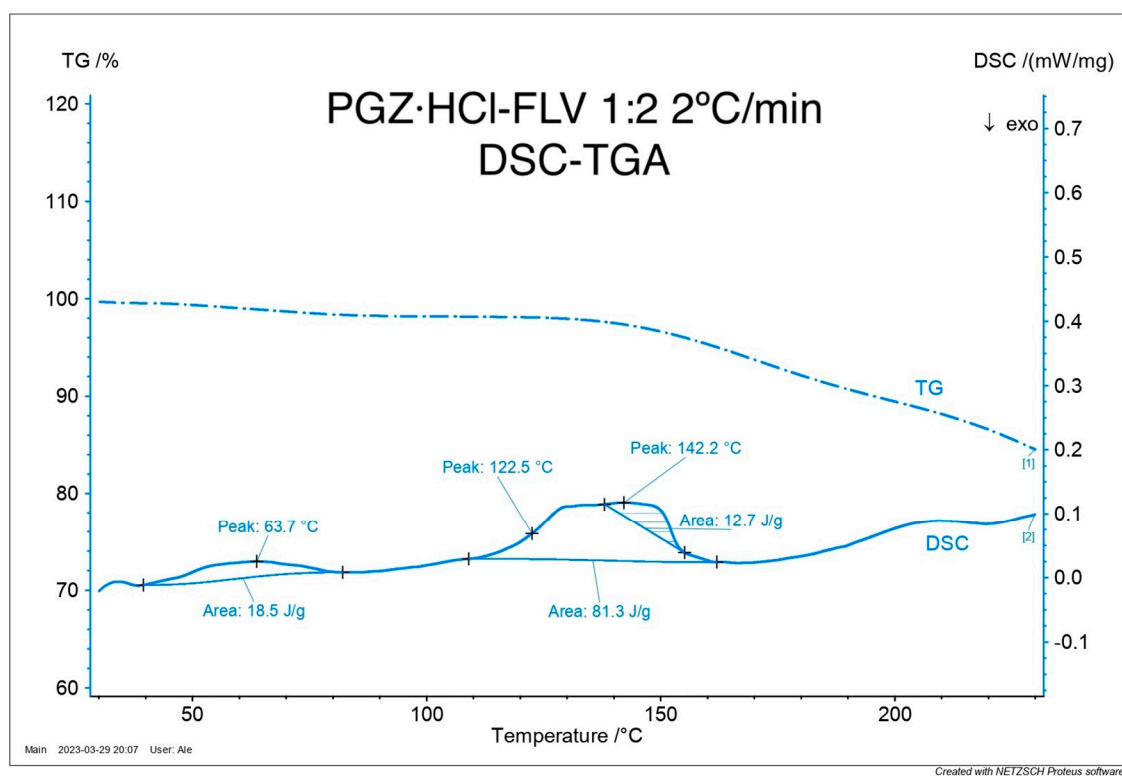
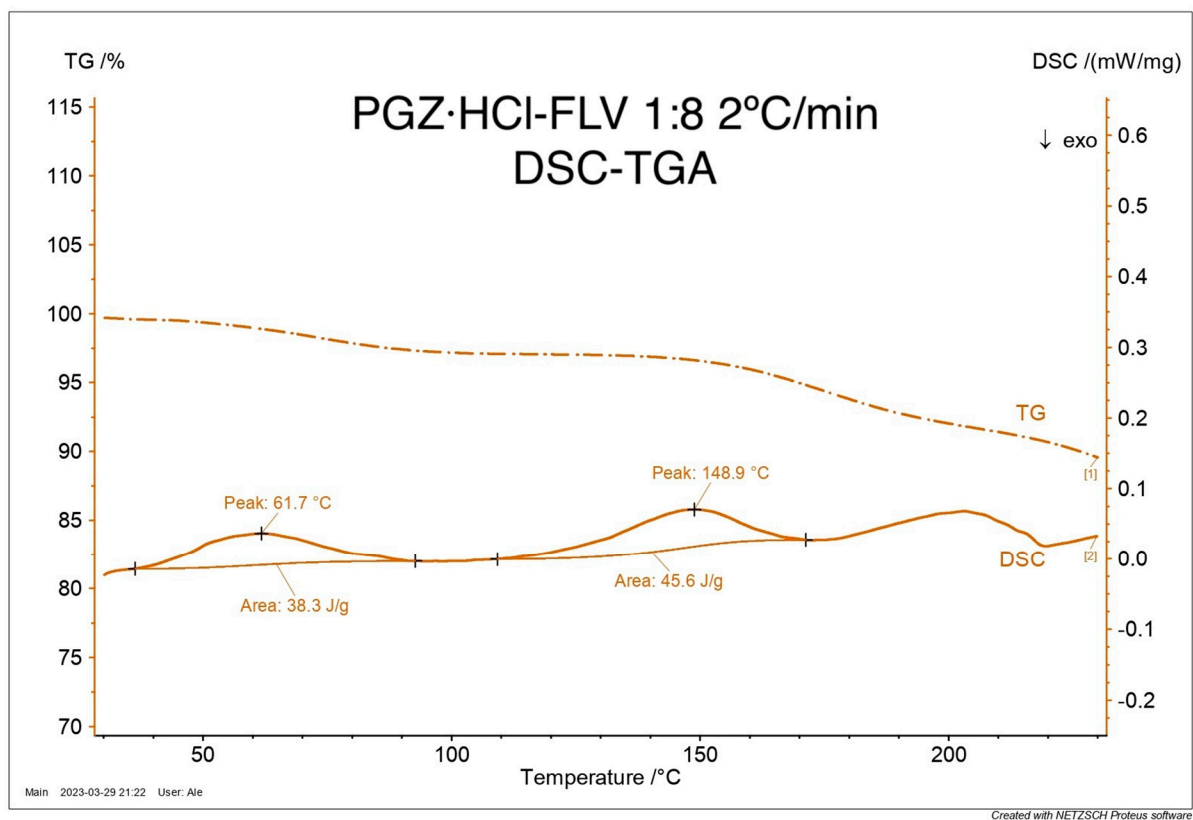
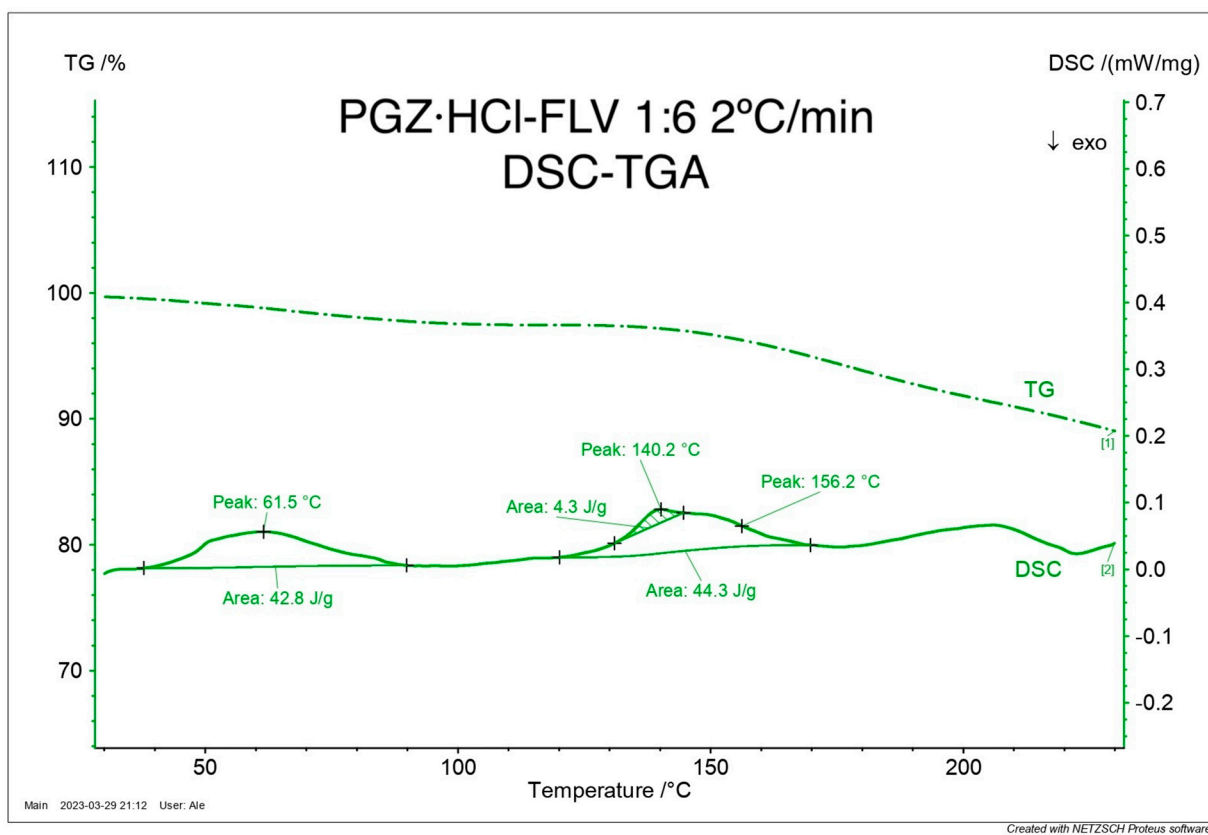
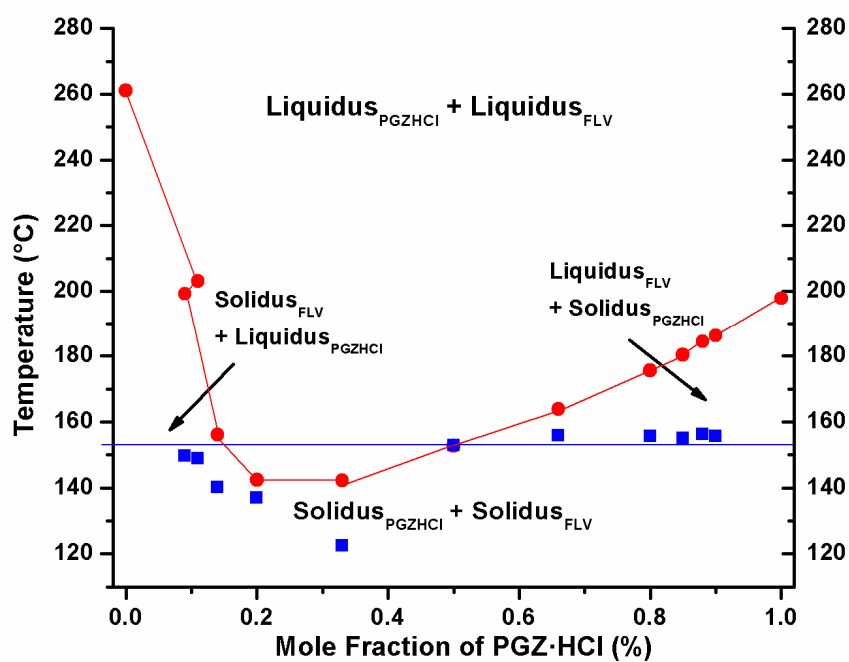
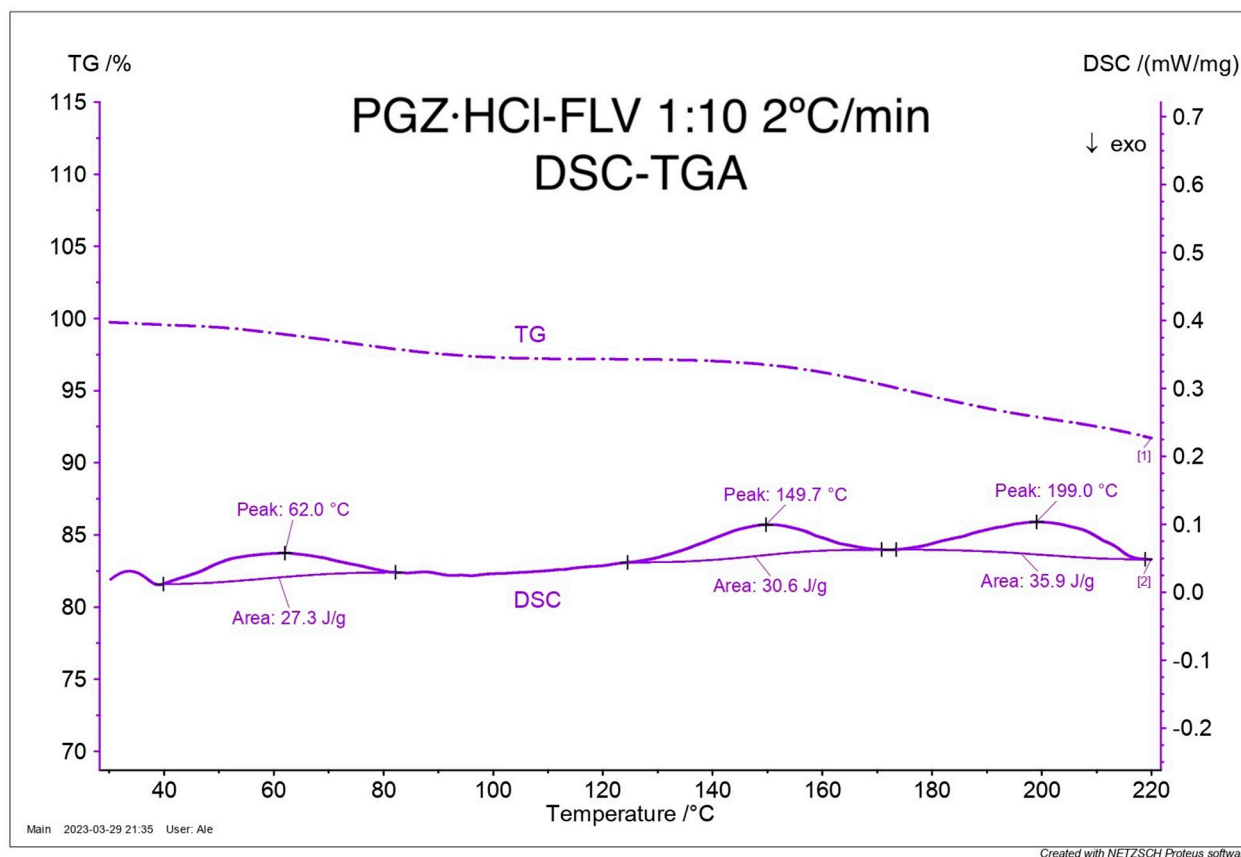


Figure SM11. Full FT-IR spectra of the solid forms of PGZ·HCl-FLV at different stoichiometric ratios (2:1; 4:1; 6:1; 8:1 and 10:1)









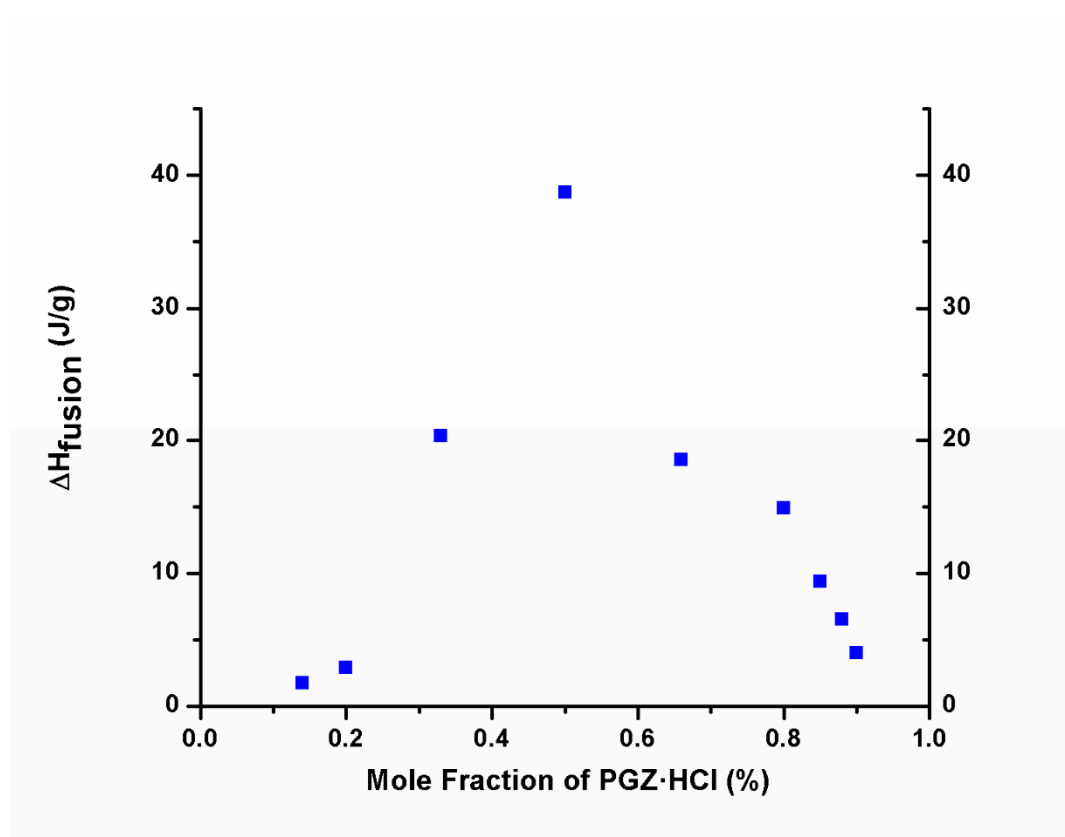
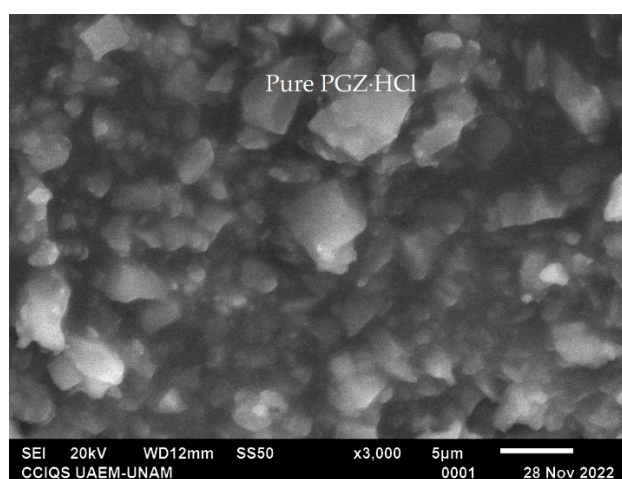
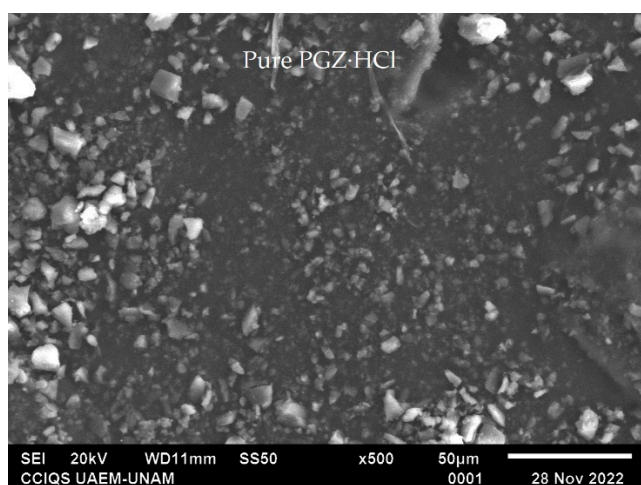
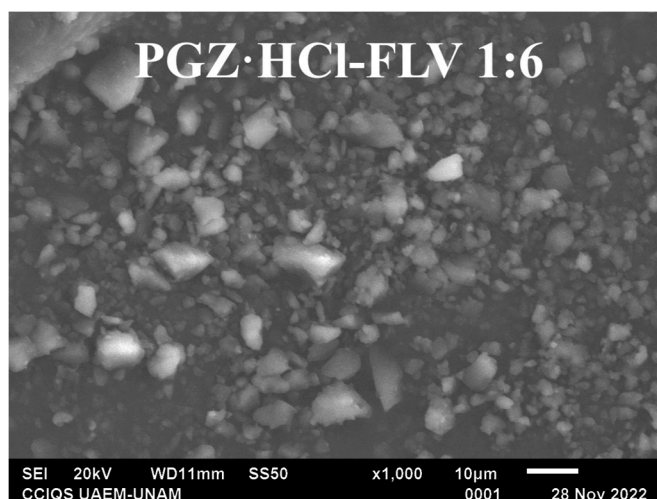
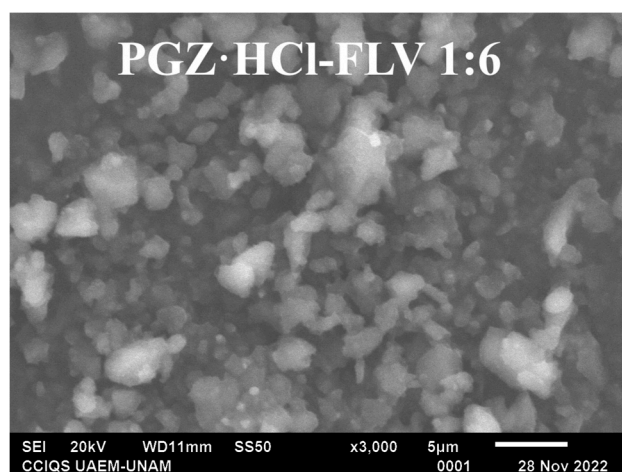
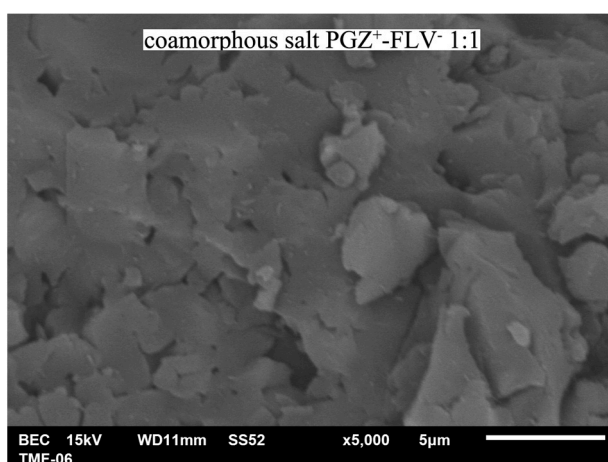
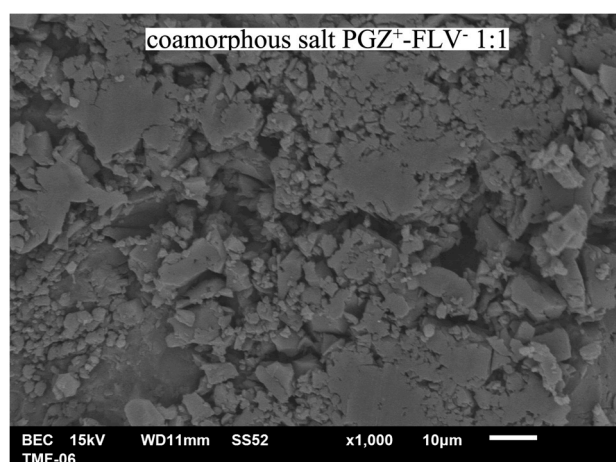
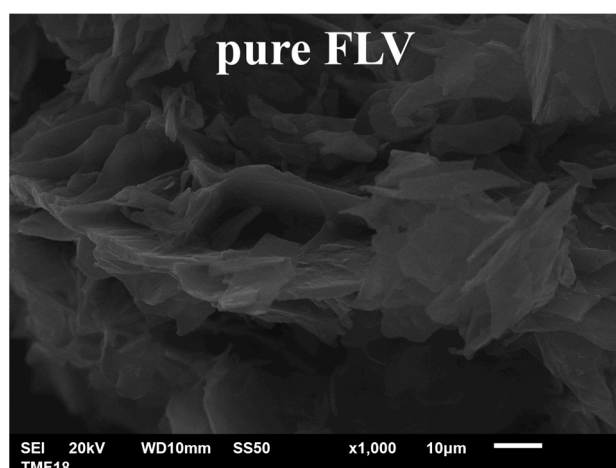
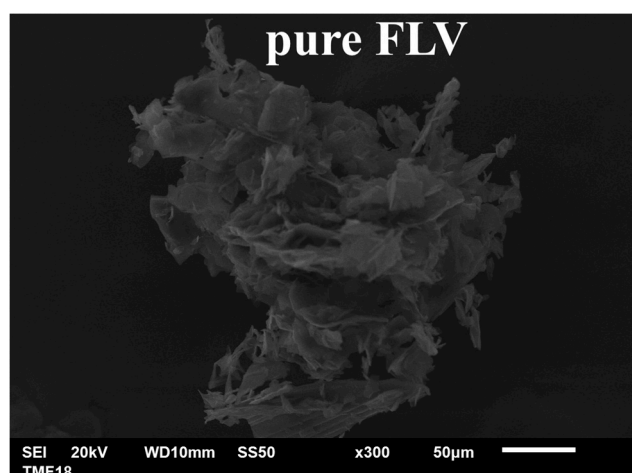


Figure SM12. PGZ-HCl-FLV binary phase diagram and Tammann's plot triangle. Thermograms corresponding to the molar ratios 1:1; 1:2; 1:4; 1:6; 1: and 1:10 at 2 °C/min.





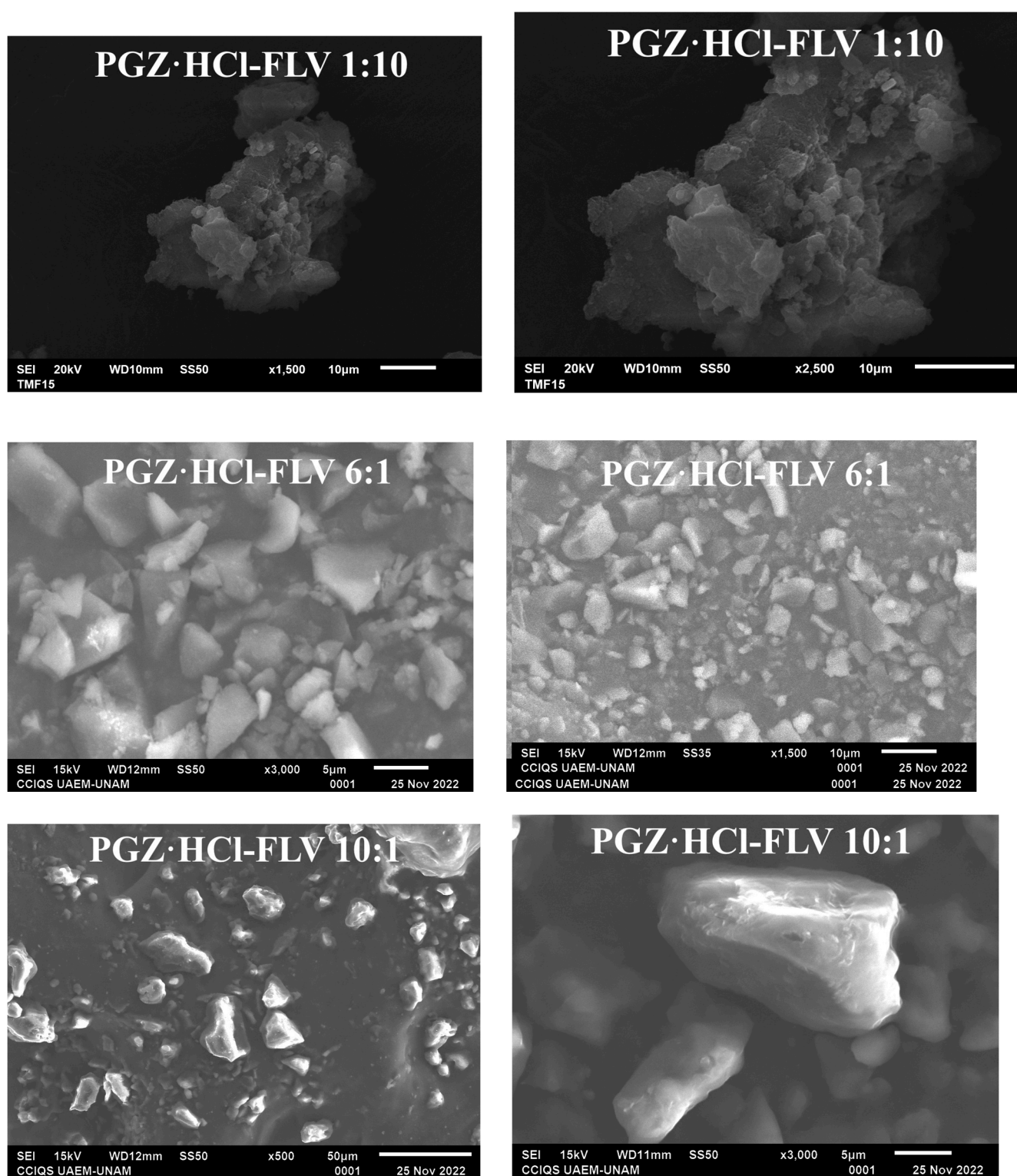


Figure SM13. Grain morphology images of the solid forms (1:1; 1:6; 1:10; 6:1; and 10:1)

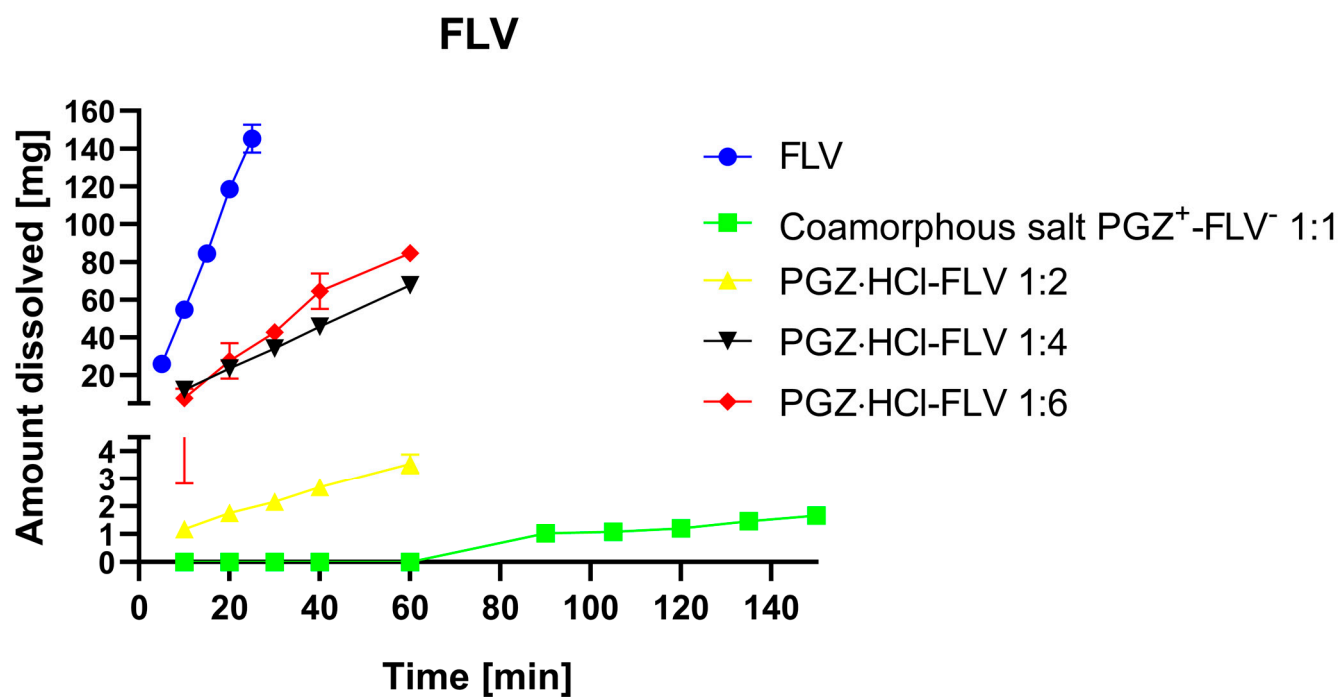


Figure SM14. Dissolution profiles with another scale on the y-axis show the plots in more detail.